Energy Dissipation in Solids due to Material Inelasticity, Viscous Coupling, and Algorithmic Damping

Han Yang[1], Hexiang Wang[2], Yuan Feng[3], Fangbo Wang, Ph.D.[4], and Boris Jeremić, Ph.D.[5]

[1]Department of Civil and Environmental Engineering, University of California, Davis, CA, USA.
[2]Department of Civil and Environmental Engineering, University of California, Davis, CA, USA.
[3]Department of Civil and Environmental Engineering, University of California, Davis, CA, USA.
[4]Department of Civil and Environmental Engineering, University of California, Davis, CA, USA.
[5]Department of Civil and Environmental Engineering, University of California, Davis, CA, USA.

ABSTRACT

Presented is a study on energy dissipation in dynamic inelastic systems due to material inelasticity, viscous damping, and algorithmic damping. Formulation for plastic dissipation is based on thermodynamics, with consideration of plastic free energy. Computation of viscous energy dissipation of the Rayleigh type is developed and discussed. Energy dissipation due to algorithmic damping is discussed as well, and compared with previous two, physical energy dissipation mechanisms. Energy dissipation due to all three dissipation mechanisms are illustrated and discussed in relation to single element tests and dynamic wave propagation problems.

INTRODUCTION

Numerical simulation of inelastic dynamic solid systems has three mechanisms of energy dissipation:

- Material inelasticity, hysteretic damping,
- Viscous coupling between solid and fluid (external or internal),
- Algorithmic, numerical damping.

The first two energy dissipation mechanisms have physical interpretations, while the last mechanism is primarily due to numerical integration of dynamic equations of motion.

Energy dissipation from inelasticity and viscous effects is physically correct if properly modeled and calibrated. Energy dissipation can also be used to improve performance and optimize engineering design. Proper modeling of different energy dissipation mechanics provides insight into realistic response of engineering solids. Substituting one mechanism of energy dissipation with another one might not provide proper insight into realistic response of engineering solids.

The mechanical energy that irreversibly transforms into heat in inelastic materials is defined as the energy dissipation due to material inelasticity, or simply referred to as plastic energy dissipation. This energy dissipation mechanism is dominant for any significant static or dynamic loading, that leads to yielding and material damage. Plastic energy dissipation is displacement proportional (Argyris and Mlejnek 1991).

The proper modeling of plastic energy dissipation in inelastic solids was presented earlier (Yang et al. 2018b). The difference between plastic energy dissipation and plastic work, which was first described by Farren and Taylor (1925), was addressed with focus on the accurate computation of plastic free energy and plastic dissipation in different inelastic material models. Plastic energy dissipation modeling and experiments are discussed in a number of recent papers (Mason et al. 1994; Collins and Houlsby 1997; Rittel 2000; Rittel and Rabin 2000; Rosakis et al. 2000; Collins and Kelly 2002; Feigenbaum and Dafalias 2007; Veveakis et al. 2012).

The dissipative interaction between solid and viscous fluid, internal in pores of porous solid, or external to solids and structures, can also dissipate significant amount of mechanical energy. This type of dissipation is referred to as viscous energy dissipation or viscous damping. Viscous energy dissipation is velocity proportional (Argyris and Mlejnek 1991). Modeling of viscous damping without explicitly taking into account interacting solid/structure and fluid is usually done using Caughey damping (Caughey 1960). Special case of Caughey damping is Rayleigh damping, where damping matrix is obtained by a linear combination of the mass and stiffness matrices. It was pointed out by Hall (2006) that the damping forces obtained from Rayleigh damping can be

unrealistically high. This makes the analysis result nonconservative, and require careful calibration of damping parameters.

Sometimes high level of Rayleigh damping is used to mimic inelastic material behavior. In other words, material nonlinear/inelastic behavior is modeled using linear elastic material and non-physical, high level of Rayleigh damping. It will be shown that energy dissipation using plastic dissipation and Rayleigh viscous damping lead to differences in response, particularly when significant material nonlinear/inelastic behavior is present.

Algorithmic damping, or numerical damping, is introduced into the system during time integration of equations of motion, by most commonly used time marching algorithms, for example the Newmark family algorithms (Newmark 1959; Hilber et al. 1977; Chung and Hulbert 1993). These time integration methods can be made energy conserving with proper choice of integration parameters, for example by choosing $\gamma = 0.500$ and $\beta = 0.250$ for Newmark algorithm.

However, recent studies have shown that the Newmark family of algorithm might lose its energy conserving properties in some cases, for example, geometric nonlinear problems, impact/contact problems, and large time step simulations (Krenk 2006; Krenk 2014). Efforts have been made to develop various types of energy conserving time integration algorithms (Simo and Wong 1991; Bathe 2007; Gonzalez 2000; Krenk 2014). In this study, the classic Newmark time integration algorithm is used, and no energy conserving issue mentioned earlier is observed in any of the presented cases. System energy conservation is in fact maintained in all cases when the Newmark parameter $\gamma = 0.500$ and $\beta = 0.250$. For any choice of $\gamma > 0.500$, Newmark family algorithms will dissipate, or produce energy in the elastic or inelastic system (Argyris and Mlejnek 1991; Hughes 1987). This algorithmic energy dissipation or production can have significant effect on results of modeling and simulation of a dynamic system.

It is noted that energy dissipation due to plastic dissipation and/or viscous damping and/or algorithmic damping is inherent to loading of solids and structures. Plastic dissipation is always present for yielding material, and is calculated on the constitutive level for any type of loading, monotonic or cyclic, static or transient. Viscous damping is present for transient loading only,

monotonic or cyclic, and is calculated on a single finite element level. Algorithmic damping is present for transient loading only, monotonic or cyclic, and can be calculated for a single finite element or finite element system level. Presented framework allows for detailed energy dissipation calculations for all of the above mechanisms.

The next section presents the theoretical formulations used to compute energy dissipation due to material inelasticity, Rayleigh damping, and algorithmic damping. Next, a number of numerical examples are used to illustrate the differences in displacement and energy responses when different energy dissipation mechanisms are used. Paper is concluded with a number of suggestions on the choices of energy dissipation mechanisms for dynamic modeling of inelastic solids.

ENERGY DISSIPATION MECHANISMS

Plastic Energy Dissipation

Energy dissipation due to material inelasticity is a phenomenon that can be observed in most structural and geotechnical materials during deformation. Plastic energy dissipation can be used to estimate material damage. According to the second law of thermodynamics, the energy dissipation of a system should always increase or remain constant as deformation occurs. Ability to follow energy dissipation, a scalar, during static and dynamic deformation can provide useful information about the performance of solids and structures, and can be used to improve design and/or retrofit.

Unfortunately, there exists a misconception where plastic work is used as a measure of plastic energy dissipation. This misconception originates from ignoring plastic free energy, which together with plastic dissipation makes up plastic work. Plastic free energy can make up a significant portion of plastic work, which renders energy dissipation results incorrect. The correct modeling of plastic energy dissipation follows the principles of thermodynamics, which ensures energy balance and nonnegative incremental energy dissipation. Based on the formulations derived from thermodynamics, a framework for computing plastic energy dissipation was established by Yang et al. (2018b), which is applied to the numerical examples presented in this paper.

Following the first and second laws of thermodynamics, the equation for plastic energy dissi-

pation in decoupled material models was presented by Yang et al. (2018b):

$$\Phi = \sigma_{ij}\dot{\epsilon}_{ij} - \sigma_{ij}\dot{\epsilon}^{el}_{ij} - \rho\dot{\psi}_{pl} \geq 0 \tag{1}$$

where Φ is the rate of plastic energy dissipation per unit volume, σ_{ij} is the stress tensor, ϵ_{ij} is the strain tensor, ϵ^{el}_{ij} is the elastic part of the strain tensor, ρ is the mass density of the material, ψ_{pl} is the plastic free energy per unit volume. All stresses are defined as the effective stresses. Sign convention for the stress is consistent with the standard definition in mechanics of materials, i.e. positive in tension. Note that Equation 1 holds under the assumption of isothermal process, which is a reasonable assumption for analysis of most civil engineering problems (Collins and Houlsby 1997).

For most inelastic material models, the stress σ_{ij}, total strain ϵ_{ij} and elastic strain ϵ^{el}_{ij} are parts of the standard output for the material response. A challenge is to evaluate plastic free energy ψ_{pl}, that is not defined explicitly, if at all, for many classic material models. The physical interpretation of plastic free energy is related to the state of the material's micro-structure. Physical interpretation of plastic free energy was discussed and illustrated in earlier publications (Besseling and Van Der Giessen 1994; Collins and Kelly 2002; Yang et al. 2018b; Yang et al. 2018a).

For pressure-independent inelastic material models (e.g. von Mises plasticity) with isotropic and/or kinematic hardening, the plastic free energy can be calculated from

$$\psi_{pl} = \psi^{iso}_{pl} + \psi^{kin}_{pl} = \frac{1}{2\rho\kappa_1}k^2 + \frac{1}{2\rho a_1}\alpha_{ij}\alpha_{ij} \tag{2}$$

where the plastic free energy ψ_{pl} is decomposed into two parts that are related to isotropic hardening ψ^{iso}_{pl} and kinematic hardening ψ^{kin}_{pl}. Here scalar k is the size of the yield surface and tensor α_{ij} is the back stress tensor representing the center of the yield surface, while κ and a_1 are nonnegative material constants.

Rayleigh Damping

To compute the energy dissipation due to viscous damping, we start with the general form of the equation of motion:

$$M_{ij}\ddot{u}_j(t) + C_{ij}\dot{u}_j(t) + K_{ij}^{elpl}(t)u_j(t) = f_i(t) \tag{3}$$

where $u_j(t)$ is the vector of generalized displacements, M_{ij} is the mass matrix, C_{ij} is the damping matrix, $K_{ij}^{elpl}(t)$ is the inelastic stiffness matrix that generally evolves with time, $f_i(t)$ is the external load vector. For linear viscous damping of the Rayleigh type, the damping matrix is expressed as

$$C_{ij} = a_M M_{ij} + a_K K_{ij}^{el} \tag{4}$$

where a_M and a_K are damping constants with units of s^{-1} and s, respectively. The stiffness matrix used to construct the damping matrix is usually the initial tangent stiffness matrix, which is also the elastic stiffness K_{ij}^{el} for inelastic materials. Equation 4 indicates that the damping matrix C_{ij} is constant through the entire simulation.

The expression used to compute the damping constants for a desired damping ratio ξ in a specified frequency range from $\hat{\omega}$ to $R\hat{\omega}$ was given by Hall (2006) as

$$a_M = 2\xi\hat{\omega}\frac{2R}{1+R+2\sqrt{R}} \quad , \quad a_K = 2\xi\frac{1}{\hat{\omega}}\frac{2}{1+R+2\sqrt{R}} \tag{5}$$

It can be seen in Equation 4 that there are mass-proportional and stiffness-proportional parts in Rayleigh damping. The combination of mass-proportional and stiffness-proportional damping can provide a desired control over modal damping ratios. However, as pointed out by Hall (2006), classic Rayleigh damping must be used with appropriate damping coefficients, which should give a near-constant value of damping for all modes with frequencies that are of interest. For the modes outside the prescribed frequency range, the damping ratios are unrealistically high.

The incremental form of energy balance for a dynamic system with viscous damping can be

expressed as

$$\Delta W_{Input} = \Delta E_K + \Delta D_V + \Delta W_M \tag{6}$$

The left hand side of Equation 6 is the increment of external input work

$$\Delta W_{Input} = f_i \Delta u_i \tag{7}$$

The three terms on the right hand side of Equation 6 are the increment of kinetic energy ΔE_K, the increment of viscous energy dissipation ΔD_V, and the increment of material work of the system ΔW_M

$$\begin{aligned} \Delta E_K &= M_{ij} \ddot{u}_j \Delta u_i \\ \Delta D_V &= C_{ij} \dot{u}_j \Delta u_i \\ \Delta W_M &= K_{ij}^{elpl} u_j \Delta u_i = \Delta E_S + \Delta E_P + \Delta D_P \end{aligned} \tag{8}$$

Note that the term of material work W_M can be separated into an elastic part and a plastic part. These two components are known as the elastic strain energy E_S and the plastic work of the system, respectively. Then, as mentioned in the previous section, plastic work can be further decomposed into plastic free energy E_P and plastic energy dissipation D_P.

Algorithmic Energy Dissipation

Newmark time integration method (Newmark 1959) is used for all cases in this study. The forward displacements ${}^{n+1}u_i$ and velocities ${}^{n+1}\dot{u}_i$ are expressed in terms of their current values and the forward and current values of the acceleration

$$\begin{aligned} {}^{n+1}\dot{u}_i &= {}^{n}\dot{u}_i + (1-\gamma) h \, {}^{n}\ddot{u}_i + \gamma h \, {}^{n+1}\ddot{u}_i \\ {}^{n+1}u_i &= {}^{n}u_i + h \, {}^{n}\dot{u}_i + (\frac{1}{2} - \beta) h^2 \, {}^{n}\ddot{u}_i + \beta h^2 \, {}^{n+1}\ddot{u}_i \end{aligned} \tag{9}$$

where Δt is the length of each time step, γ and β are the Newmark integration parameters that controls the amount of algorithmic damping in the system.

Krenk (2006) gave the incremental form of the energy balance equation 6 over increment t_n to

167 t_{n+1}, for Newmark algorithm

$$
\begin{aligned}
&\left[\frac{1}{2}M^{\star}_{ij}\dot{u}_i\dot{u}_j + \frac{1}{2}K_{ij}u_iu_j + \left(\beta - \frac{1}{2}\gamma\right)\frac{1}{2}h^2M^{\star}_{ij}\ddot{u}_i\ddot{u}_j\right]\Bigg|_{t_n}^{t_{n+1}} = \\
&\quad + \Delta u_i\left[\frac{1}{2}(f_i^{n+1} + f_i^n) + \left(\gamma - \frac{1}{2}\right)\Delta f_i\right] \\
&\quad - \left(\gamma - \frac{1}{2}\right)\left[K_{ij}\Delta u_i\Delta u_j + \left(\beta - \frac{1}{2}\gamma\right)h^2M^{\star}_{ij}\Delta\ddot{u}_i\Delta\ddot{u}_j\right] \\
&\quad - \frac{1}{2}h\left[h^{-2}C_{ij}\Delta u_i\Delta u_j + \frac{1}{4}C_{ij}(\dot{u}_i^{n+1} + \dot{u}_i^n)(\dot{u}_j^{n+1} + \dot{u}_j^n)\right] \\
&\quad + \frac{1}{2}\left(\beta - \frac{1}{2}\gamma\right)^2 h^3C_{ij}\Delta\ddot{u}_i\Delta\ddot{u}_j
\end{aligned}
\tag{10}
$$

169 where the equivalent mass matrix $M^{\star}_{ij}$ is defined as

$$
M^{\star}_{ij} = M_{ij} + \left(\gamma - \frac{1}{2}\right)hC_{ij} \tag{11}
$$

171 Rearranging Equation 10 gives the explicit expression for the amount of algorithmic energy
172 dissipation over an increment

$$
\begin{aligned}
&\left[E_K + D_V + W_M - W_{Input}\right]_{t_n}^{t_{n+1}} = \\
&\quad + \left(\gamma - \frac{1}{2}\right)\Delta f_i\Delta u_i + \frac{1}{2}\left(\beta - \frac{1}{2}\gamma\right)^2 h^3C_{ij}\Delta\ddot{u}_i\Delta\ddot{u}_j \\
&\quad - \left(\gamma - \frac{1}{2}\right)\left[K_{ij}\Delta u_i\Delta u_j + \left(\beta - \frac{1}{2}\gamma\right)h^2M^{\star}_{ij}\Delta\ddot{u}_i\Delta\ddot{u}_j\right] \\
&\quad - \left[\frac{1}{2}\left(\gamma - \frac{1}{2}\right)hC_{ij}\dot{u}_i\dot{u}_j + \left(\beta - \frac{1}{2}\gamma\right)\frac{1}{2}h^2M^{\star}_{ij}\ddot{u}_i\ddot{u}_j\right]\Bigg|_{t_n}^{t_{n+1}}
\end{aligned}
\tag{12}
$$

174 When $\gamma = 0.500$ and $\beta = 0.250$, all the terms on the right hand side of Equation 12 vanish, thus no
175 algorithmic energy dissipation exists. For other values of γ and β, algorithmic energy dissipation,
176 or even energy production, is observed in the system.

177 NUMERICAL EXAMPLES

178 Numerical simulations presented in this paper are performed using the MS ESSI Simulator

system (Jeremić et al. 2018), and all the examples presented here are available at http://ms-essi.info/. Energy dissipation due to material inelasticity and Rayleigh damping is investigated through a series of single-element tests with different material parameters and loading conditions. Then, elastic and inelastic materials are used in a stack of solid brick elements model to further illustrate energy dissipation in wave propagation problems. Finally, cases with plastic energy dissipation, Rayleigh damping, and algorithmic damping are analyzed to demonstrate the importance of energy dissipation mechanisms in dynamic finite element modeling.

The inelastic material model used in this study is associated von Mises plasticity with nonlinear Armstrong-Frederick kinematic hardening. The yield function of von Mises plasticity is

$$f = \sqrt{(s_{ij} - \alpha_{ij})(s_{ij} - \alpha_{ij})} - \sqrt{\frac{2}{3}}k \tag{13}$$

The general expression for Armstrong-Frederick kinematic hardening rule is

$$d\alpha_{ij} = \frac{2}{3}h_a d\epsilon_{ij}^{pl} - \sqrt{\frac{2}{3}}c_r d\lambda \alpha_{ij} \tag{14}$$

where $d\lambda$ is a nonnegative scalar plastic multiplier and h_a and c_r are nonnegative material hardening constants. The parameter h_a controls the initial stiffness of the material after yielding, while ratio h_a/c_r controls the limit of stress magnitude, or shear strength.

For all dynamic problems analyzed, Newmark integration algorithm is used. In most cases with elasticity and inelasticity and Rayleigh damping, the numerical integration parameters are chosen in a way so that no algorithmic damping exists in the system, i.e. Newmark parameters $\gamma = 0.500$ and $\beta = 0.250$. Only for the last example, algorithmic damping was used, by choosing Newmark parameters $\gamma > 0.500$ and $\beta = 0.250(\gamma + 0.500)^2$.

External loads are applied incrementally using load- or displacement-control scheme. Nonlinear system of equations is solved using Newton-Raphson algorithm with line searching to help convergence. Standard 8-node-brick elements are used in all examples.

Single Element Tests

Energy dissipation in single 8-node-brick element is studied in this section. The individual and combined effects of material inelasticity and Rayleigh damping are investigated through a series of numerical examples.

The single element model, with boundary conditions and loads, is shown in Fig.1. During the shearing stage, the bottom of the element is fixed and imposed motion is applied on the top. The main reason for using displacement-control scheme is to eliminate any resonance effects that might occur during faster dynamic tests, if load-control is used. The time increment Δt for the Newmark algorithm is set to $\Delta t = 0.01$s.

Elastic Material without Rayleigh Damping

The first example uses linear elastic material with no Rayleigh damping. No energy dissipation in any form is expected in this case. The equivalence between external work and mechanical energy stored in the system (energy balance) in single-element model is verified through this example.

The material properties used for this case are summarized in Table 1.

Fig.2 shows the displacement, stress-strain, and energy responses of the case using linear elastic material without Rayleigh damping. The stress-strain response indicates that the material is linear elastic, which is expected. Only kinetic energy and strain energy appear in this example since there is no energy dissipation. Notice that the kinetic energy is not zero at the beginning because of the initial velocity that comes with the sine-wave imposed motion.

The comparison between external work, which is computed using the imposed displacement time series and nodal force response, and total mechanical energy stored in the system, calculated at each Gauss point, shows that energy balance is achieved. Note that the frequency of oscillation of energy curves, shown in Fig.2(c)(d), is twice of that of the displacement time series, Fig.2(a). This is expected for linear elastic systems under displacement control loading.

Inelastic Material without Rayleigh Damping

The next example focuses on the energy dissipation due to material inelasticity only. A more systematic study of plastic energy dissipation in solids can be found in Yang et al. (2018b), where the

energy dissipation behavior of various inelastic material models was investigated. In this section, a material model defined with von Mises yield function and Armstrong-Frederick nonlinear kinematic hardening is used. No Rayleigh damping is added to any model in this section.

Table 2 summarizes material parameters for these studies. Three materials with the same shear strength, controlled by ratio h_a/c_r, but different post-yield stiffness, h_a, are modeled. These three materials are used in single element examples and wave propagation problems. They will be referred to as soft, medium, and hard inelastic materials in the remaining parts of this paper. Fig.3 shows the stress-strain response and energy computation results for the cases using inelastic material and no Rayleigh damping.

According to Fig.3, by keeping shear strength constant and increase post-yield stiffness, the amount of plastic energy dissipation increases. This is consistent with the stress-strain response which shows that the degree of plastification increases as the parameter h_a increases. It is also noted that changes in strain energy during cyclic shearing, is very small, due to a small elastic region of the material model.

Elastic Material with Rayleigh Damping

The next example focuses on the energy dissipation due to viscous damping. Viscous damping is modeled using Rayleigh damping. Linear elastic material is used in all cases in this section so that energy dissipation can only be caused by Rayleigh damping.

Energy dissipation by Rayleigh damping can be analyzed using equations presented in section 2. By substituting the expression of Rayleigh damping matrix (Equation 4 and 5) into the term of viscous energy dissipation in Equation 8, one obtains

$$\Delta D_V = C_{ij}\dot{u}_j\Delta u_i = \frac{4\xi}{1+R+2\sqrt{R}}\left(\hat{\omega}RM_{ij} + \frac{K^{el}_{ij}}{\hat{\omega}}\right)\dot{u}_j\Delta u_i \tag{15}$$

Table 3 shows the parameters used in this section. The effect of damping ratio ξ to the amount of viscous energy dissipation is investigated. Typical values of damping ratio ξ for soils and structures are selected. The lower limit of damping range $\hat{\omega}$ can be computed from the model's fundamental

frequency ω_1. It is common practice to set $\hat{\omega} = (2/3)\omega_1 = (4\pi)/(3T_1)$ due to nonlinear response of the system (Hall 2006). In order to cover the frequency range from $(2/3)\omega_1$ to $3\omega_1$, a second-mode frequency of a linear shear beam, the parameter R should be set to 4.5. For the examples in this section, R is chosen to be slightly larger, $R = 5.0$, to cover a larger range.

The energy computation results are shown in Fig.4. It can be observed that the viscous energy dissipation increases as the damping ratio increases. The values indicate a linear relationship between the viscous energy dissipation and damping ratio, that is consistent with Equation 15. All other forms of energy are the same in these cases.

Inelastic Material with Rayleigh Damping

In the previous examples, the separate effects of material inelasticity and Rayleigh damping have been studied. In this example, both energy dissipation mechanisms, inelasticity and Rayleigh damping, are used. In particular, it will be shown that the relative amount of energy dissipation due to these two mechanisms is very sensitive to the choice of material and damping parameters.

Fig.5 shows the stress-strain response and energy computation results for the three cases using inelastic material model with Rayleigh damping. As can be observed, energy dissipation results are very different in these three cases. Plastic energy dissipation can be much larger or much smaller or very similar to the viscous energy dissipation, depending on the choices of simulation parameters. More discussion on the combined effect of plastic energy dissipation and Rayleigh damping is shown in section 3 where a wave propagation problem is studied.

Wave Propagation

The numerical examples for a single-element present a fundamental understanding of the energy behavior for a fully controlled system, with fixed and prescribed displacements. In this section, the energy dissipation due to material inelasticity and viscous damping in a wave propagation problem is investigated. Compared to the single-element cases where energy transformation happens in one element, the wave propagation problem can illustrate the evolution of energy storage and dissipation in time and space.

It is important to select appropriate grid-spacing and time-step size to ensure numerical stability

and accuracy. A detailed study on the discretization effects in the finite element simulation of seismic waves in elastic and inelastic media was conducted by Watanabe et al. (2017). According to Jeremić et al. (2009), the suitable maximum grid spacing Δx for shear wave propagation for a model using eight-node-brick finite elements can be determined by considering shear wave velocity V_s, and the highest frequency of the input signal f_{max}:

$$\Delta x \leq \frac{V_s}{10 f_{max}} \tag{16}$$

The time-step size Δt in wave propagation problem is usually chosen on the basis that a given wave front does not reach two consecutive nodes at the same time. The following condition, given by Watanabe et al. (2017), is used to ensure numerical stability when using Newmark time integration algorithm:

$$\Delta t \leq \frac{\Delta x}{V_s} \tag{17}$$

The model used in this section is a stack of 8-node-brick elements, as shown in Fig.6. It is noted that for inelastic material models, where shear stiffness is reduced due to inelasticity, as is the case here, Equation 16 should still hold. This means that the element size has to be small enough so that the model is capable of propagating waves through inelastic material. However, there is a limit of how small the mesh size can become, and what frequencies can be accurately propagated. For a given example, assuming reduction of shear stiffness, shear wave velocity, from $V_s = 400$m/s (elastic) to $V_s = 40$m/s (inelastic). Then, based on Equation 16, the length of each element is chosen to be $\Delta x = 1$m. Meanwhile, according to Equation 17, the time increment Δt for the Newmark algorithm is set to $\Delta t = 0.001$s.

Model features a total of 4000 eight-node-brick elements, with boundary conditions that allow only shear waves to propagate. The left 3900 elements are used to model a layer of material that is assumed to remain elastic during wave propagation. The material model properties of the elastic layer was given in Table 1. The right 100 elements represent a layer that can be elastic or inelastic. In some examples, this layer remains elastic, in order to investigate the effect of Rayleigh damping.

In other examples, this layer is inelastic, and dissipates energy through material inelasticity and/or Rayleigh damping.

An Ormsby wavelet (Ryan 1994), with peak value controlled by A and frequency contents starting from f_1 to f_4, with a constant amplitude from f_2 to f_3, is imposed to the fixed end of the model. The function of Ormsby wavelet is

$$\begin{aligned} f(t) =& A\left[\left(\frac{\pi {f_4}^2}{f_4-f_3} sinc(\pi f_4(t-t_s))^2 - \frac{\pi {f_3}^2}{f_4-f_3} sinc(\pi f_3(t-t_s))^2\right)\right. \\ & \left. - \left(\frac{\pi {f_2}^2}{f_2-f_1} sinc(\pi f_2(t-t_s))^2 - \frac{\pi {f_1}^2}{f_2-f_1} sinc(\pi f_1(t-t_s))^2\right)\right] \end{aligned} \tag{18}$$

where t_s is the time when maximum amplitude is occurring, and sine cardinal is defined as $sinc(x) = sin(x)/x$. Please note that from Equation 18, peak value f^{peak} is defined at $t = t_s$ as

$$f^{peak} = A\pi\left(f_4 + f_3 - f_2 - f_1\right) \tag{19}$$

Fig.7 shows the imposed displacement, in time domain and frequency domain, created using Ormsby wavelet with $A = 0.01$m·s, $f_1 = 1.0$Hz, $f_2 = 2.0$Hz, $f_3 = 4.0$Hz, and $f_4 = 5.0$Hz.

Elastic Material without Rayleigh Damping

In the first case, material parameters for elastic material are used for the entire model. This simple setup illustrates the energy transformation process as shear waves propagate and reflect within a uniform media.

Fig.8 shows the displacement response at the free end of the model in time and frequency domain, as well as the energy and stress-strain results, for the case of wave propagation within an uniform media. As expected, the displacement at the free end is twice in magnitude and same in frequency contents. The stress-strain response of the material is a straight line since linear elastic material is used in this case.

Because of the absence of energy dissipation mechanism, the total mechanical energy remains constant after the wave is input into the system. The transformation between kinetic energy and

strain energy is observed when the shear wave hits the free end of the model and gets reflected back. During the wave propagation process, before and after the reflection, the amounts of kinetic energy and strain energy are exactly the same, which is expected in a wave propagation problem.

Elastic and Inelastic Material without Rayleigh Damping

In this section, the energy dissipation due to material inelasticity during wave propagation is investigated. The inelastic material model uses von Mises yield function in combination with Armstrong-Frederick kinematic hardening. Soft, medium, and hard inelastic materials, shown in Table 2 on page 26, are used to investigate the influence of post-yield stiffness on plastic dissipation.

Fig.9, 10, and 11 show the displacement response at the free end of the model in time and frequency domain, as well as the stress-strain and energy results, for the cases with material inelasticity and no Rayleigh damping. Peak displacement response at the free end of the model is larger when the inelastic material is stiffer after yield. Due to the use of inelastic material, permanent deformation is observed in the displacement time series. This leads to the low frequency contents in the displacement spectrum.

According to the energy plots, more energy is dissipated due to material inelasticity when the inelastic material has a larger post-yield stiffness. This observation is consistent with the findings from single element examples (section 3) that harder inelastic material has more plastic dissipation. When the inelastic layer is much softer than the elastic layer, the majority of the incoming wave is reflected back at the material interface instead of entering the inelastic layer. As a result, energy dissipation and displacement response are less significant in the case of a softer inelastic material.

Elastic Material with Rayleigh Damping

The next section focuses on the effect of Rayleigh damping in wave propagation problems. Linear elastic material, shown in Table 1, is used in order to only have viscous dissipation mechanism. Due to the use of Rayleigh damping, it is expected to observe viscous energy dissipation and displacement reduction throughout the model. Parametric study on the damping coefficient ξ is performed. The damping parameters used in this section are summarized in Table 4.

Fig.12, 13, and 14 show the displacement response in time and frequency domain, as well as

the energy results, when different values of damping ratio ξ are used. As expected, the amount of surface displacement reduction and energy dissipation increases when larger ξ is used. Despite changes in the peak value, the frequency contents of the displacement response at the free end remain the same as those of the input motion.

For structural materials like steel and concrete, the Rayleigh damping ratio is usually chosen to be between 0.02 to 0.05. As seen in Fig.13, about half of the input energy is dissipated due to Rayleigh damping when ξ is 0.05. It is noted that sometimes large Rayleigh damping ratio are used, as high as 0.20. These high Rayleigh damping ratios lead to a significant amount of energy dissipation through viscous energy dissipation mechanism. Such high level of energy dissipation may not be physical and will lead to underestimation of the system response.

Comparison between Plastic Dissipation and Viscous Damping

As previously noted, sometimes Rayleigh damping of the system is set to a high level to mimic inelastic material behavior. By comparing the example using soft inelastic material without Rayleigh damping, shown in Fig.9, with the one using linear elastic material and Rayleigh damping $\xi = 0.05$, shown in Fig.13, it appears that the amounts of energy dissipation are similar in these two examples. However, this correspondence is very sensitive to material properties, damping parameters, loading conditions and frequency of loading. In this section, the two examples with different energy dissipation mechanisms are reanalyzed using an input motion with different frequency content, $f_1 = 0.5$Hz, $f_2 = 1.0$Hz, $f_3 = 3.0$Hz, and $f_4 = 3.5$Hz, as shown in Fig.15.

Fig.16 shows the displacement responses and energy computation results for the two examples using different energy dissipation mechanisms. The first case uses soft inelastic material, shown in Table 2 on page 26, with no Rayleigh damping, while the second case uses linear elastic material with Rayleigh damping $\xi = 0.05$. From Fig.16, it can be seen that the amounts of energy dissipation are very different in these two cases with the new input motion. Thus, material inelasticity and viscous damping may give equal, similar amounts of energy dissipation for a specific set of simulation parameters and loading conditions, but this similarity will not hold if the model is subject to a different loading. In other words, plastic dissipation and viscous energy dissipation are not

interchangeable energy dissipation mechanisms, and should always be considered independently. Moreover, viscous damping assumes that each node of the finite element model is connected to a viscous damper, while in reality for civil engineering solids and structures most energy is not dissipated in the form of linear viscous damping (Ostadan et al. 2004; Hall 2006).

It should also be pointed out that the response, especially in the frequency domain, are very different when comparing the examples using inelastic material with the ones using only Rayleigh damping. Permanent deformation and change of stiffness, which can only be modeled with inelastic materials, are not observed in the cases using linear elastic material with Rayleigh damping. For the cases using inelastic materials, the displacement response contains frequencies that are both higher and lower than those of the input motion. For practical engineering designs, if only elastic material is used in numerical simulations, these important high frequency motions and permanent deformations could be missed completely.

Combined Effects of Plastic Dissipation and Viscous Damping

In this section, the combined effect of energy dissipation through material inelasticity and Rayleigh damping is presented. Three cases with different combinations of inelastic materials (Table 2) and damping coefficients (ξ = 0.02, 0.04, or 0.10) are simulated and analyzed. Fig.17, 18, and 19 show the displacement, stress-strain, and energy results of these three cases with both material inelasticity and Rayleigh damping. Permanent deformation and low frequency response at the free end is observed. Note that the high frequency content of motions is significantly reduced because of the Rayleigh damping in the system.

Depending on the choices of simulation parameters, it is shown that the amount of energy dissipation due to material inelasticity can be larger, smaller, or comparable to that caused by Rayleigh damping. For problems where significant solid-fluid interaction is expected, e.g. underground structure in saturated soil, the viscous damping of the soil structure interaction (SSI) system is likely to have significant contribution to energy dissipation. For other problems with little solid-fluid interaction, but large material damage, e.g. aboveground structure suffering large seismic loading, more energy is likely to be be dissipated due to material inelasticity. Thus it is

important to model not only the correct amount of energy dissipation of a system but the proper energy dissipation mechanisms as well. The system response can be very different, as shown, when different combinations of energy dissipation mechanisms are used.

Influence of Algorithmic Damping

Algorithmic damping was excluded in all previously presented examples by setting the Newmark parameter to $\gamma = 0.500$ and $\beta = 0.250$ (Hughes 1987). In practice, Newmark parameters γ and β are usually set to $\gamma > 0.500$ and $\beta = 0.250(\gamma + 0.500)^2$ in order to introduce algorithmic damping into the system. To illustrate the influence of Newmark parameters γ and β on energy dissipation, two sets of examples with algorithmic damping are analyzed.

Fig.20 and 21 show the displacement, stress-strain, and energy results of two cases where linear elastic material and no Rayleigh damping is used, which means that only algorithmic damping dissipates system energy. There is a noticeable amount of algorithmic damping when the Newmark parameters are increased to $\gamma = 0.505$ and $\beta = 0.253$. As Newmark parameters are increased to $\gamma = 0.700$ and $\beta = 0.360$, it is observed that the algorithmic damping in the system becomes unrealistically high. More importantly, most of the mechanical energy propagated by the wave is numerically dissipated even before the wave reaches the free end of the column.

Combined Effects of Plastic Dissipation, Viscous Damping, and Algorithmic Damping

For realistic modeling and simulation, usually all three energy dissipation mechanisms are used. Fig.22, 23, and 24 show the displacement, stress-strain, and energy results of the three cases where plastic dissipation, Rayleigh damping, and algorithmic damping are all present. The medium inelastic material defined in Table 2 and Rayleigh damping coefficient $\xi = 0.04$ are used for all three cases. It is observed that for a relatively small Newmark parameters $\gamma = 0.505$ and $\beta = 0.253$, the amount of energy dissipation due to algorithmic damping is comparable but less than energy dissipation caused by material inelasticity and viscous damping. As Newmark parameter γ increases to $\gamma = 0.510$ and $\beta = 0.253$, algorithmic damping becomes the comparable energy dissipation mechanism in the system. Then, when Newmark parameter γ increases even higher to $\gamma = 0.550$ and $\beta = 0.276$, the motions in the system are almost completely damped out by

algorithmic damping, and material inelasticity and viscous damping do not play any significant role.

As noted by Argyris and Mlejnek (1991), high frequencies can be introduced into finite element models, during discretization process. It is thus important to be able to try to damp those unrealistic higher frequencies by applying a reasonable amount of algorithmic damping. It is noted that introduction of algorithmic damping has to be done carefully, as in some cases, as shown here, algorithmic damping can surpass all other physical forms of energy dissipation. It is thus suggested that a sensitivity study should be conducted for dynamic finite element models, so that influence of algorithmic damping on results is better understood.

CONCLUSIONS

Presented was a study on energy dissipation due to material inelasticity, Rayleigh damping, and algorithmic damping for dynamic loading of solids. The importance of proper modeling of energy dissipation due to inelastic material behavior, due to Rayleigh damping, and due to algorithmic damping in dynamic nonlinear systems was investigated and discussed. The differences in system response with these three energy dissipation mechanisms were illustrated through a series of numerical examples.

Thermomechanics formulation that correctly computes plastic energy dissipation in inelastic materials was presented. The important role of plastic free energy was emphasized. In addition, Rayleigh damping and corresponding viscous energy dissipation formulation was presented as well. Use of significant, potentially unrealistic Rayleigh damping was illustrated and discussed. This high Rayleigh damping might lead to unrealistically high energy dissipation and underestimation of the system response. Considering both plastic energy dissipation and viscous damping of the Rayleigh type, the rate form of energy balance for a dynamic system was obtained.

Presented analysis approach was illustrated using several numerical examples with energy dissipation due to material inelasticity, and/or Rayleigh damping, and/or algorithmic damping. Permanent deformation was observed in the cases using inelastic material (as expected), leading to the low frequency contents in the displacement response at the ground surface. Rayleigh damping

can significantly reduce high frequency motions, which might have important implications in evaluating the safety of structures, systems and components.

The influence of algorithmic damping was illustrated and discussed as well. Algorithmic damping mainly reduces higher frequency motions, and it exists throughout simulation process. Unrealistically high values of algorithmic damping can be obtained, and sensitivity studies are needed for proper choice of algorithmic damping parameters.

Although the amounts of dissipated energy were comparable in some cases, the observed system responses were very different when different energy dissipation mechanisms were used. All three energy dissipation mechanisms, material inelasticity, viscous damping, and algorithmic damping, model fundamentally different physical or mathematical phenomena in finite element simulation. Therefore, it is important to use appropriate energy dissipation mechanisms by following proper physics and mathematics, allowing analysts to gain confidence in obtained results, and use those results for design, assessment and retrofits.

ACKNOWLEDGMENTS

This work was supported in part by the US-DOE.

REFERENCES

Argyris, J. and Mlejnek, H.-P. (1991). *Dynamics of Structures*. North Holland in USA Elsevier.

Bathe, K.-J. (2007). "Conserving energy and momentum in nonlinear dynamics: a simple implicit time integration scheme." *Computers & structures*, 85(7), 437–445.

Besseling, J. F. and Van Der Giessen, E. (1994). *Mathematical modeling of inelastic deformation*, Vol. 5. CRC Press.

Caughey, T. (1960). "Classical normal modes in damped linear systems." *ASME Journal of Applied Mechanics*, 27, 269–271.

Chung, J. and Hulbert, G. (1993). "A time integration algorithm for structural dynamics with improved numerical dissipation: the generalized-α method." *Journal of applied mechanics*, 60(2), 371–375.

Collins, I. and Kelly, P. (2002). "A thermomechanical analysis of a family of soil models." *Geotechnique*, 52(7), 507–518.

Collins, I. F. and Houlsby, G. T. (1997). "Application of thermomechanical principles to the modelling of geotechnical materials." *Procedings of Royal Society London*, 453, 1975–2001.

Farren, W. and Taylor, G. (1925). "The heat developed during plastic extension of metals." *Proceedings of the royal society of London A: mathematical, physical and engineering sciences*, The Royal Society, 107(743), 422–451.

Feigenbaum, H. P. and Dafalias, Y. F. (2007). "Directional distortional hardening in metal plasticity within thermodynamics." *International Journal of Solids and Structures*, 44(22-23), 7526–7542.

Gonzalez, O. (2000). "Exact energy and momentum conserving algorithms for general models in nonlinear elasticity." *Computer Methods in Applied Mechanics and Engineering*, 190(13-14), 1763–1783.

Hall, J. F. (2006). "Problems encountered from the use (or misuse) of Rayleigh damping." *Earthquake engineering & structural dynamics*, 35(5), 525–545.

Hilber, H. M., Hughes, T. J. R., and Taylor, R. L. (1977). "Improved numerical dissipation for time integration algorithms in structural dynamics." *Earthquake Engineering and Structure Dynamics*,

505 5(3), 283–292.

506 Hughes, T. (1987). *The Finite Element Method ; Linear Static and Dynamic Finite Element Analysis*.
507 Prentice Hall Inc.

508 Jeremić, B., Jie, G., Cheng, Z., Tafazzoli, N., Tasiopoulou, P., Pisanò, F., Abell, J. A., Watanabe, K.,
509 Feng, Y., Sinha, S. K., Behbehani, F., Yang, H., and Wang, H. (2018). *The Real ESSI / MS ESSI*
510 *Simulator System*. University of California, Davis and Lawrence Berkeley National Laboratory.
511 http://real-essi.info/.

512 Jeremić, B., Jie, G., Preisig, M., and Tafazzoli, N. (2009). "Time domain simulation of soil–
513 foundation–structure interaction in non–uniform soils.." *Earthquake Engineering and Structural*
514 *Dynamics*, 38(5), 699–718.

515 Krenk, S. (2006). "Energy conservation in newmark based time integration algorithms." *Computer*
516 *Methods in Applied Mechanics and Engineering*, 195(44-47), 6110–6124.

517 Krenk, S. (2014). "Global format for energy-momentum based time integration in nonlinear dy-
518 namics." *International Journal for Numerical Methods in Engineering*, 100(6), 458–476.

519 Mason, J., Rosakis, A., and Ravichandran, G. (1994). "On the strain and strain rate dependence of
520 the fraction of plastic work converted to heat: an experimental study using high speed infrared
521 detectors and the kolsky bar." *Mechanics of Materials*, 17(2-3), 135–145.

522 Newmark, N. M. (1959). "A method of computation for structural dynamics." *ASCE Journal of the*
523 *Engineering Mechanics Division*, 85, 67–94.

524 Ostadan, F., Deng, N., and Roesset, J. M. (2004). "Estimating total system damping for soil-structure
525 interaction systems." *Proceedings Third UJNR Workshop on Soil-Structure Interaction,*, M. C.
526 (USGS), M. T. (USC), I. O. (BRI), and M. I. (NILIM), eds.

527 Rittel, D. (2000). "An investigation of the heat generated during cyclic loading of two glassy
528 polymers. part i: Experimental." *Mechanics of Materials*, 32(3), 131–147.

529 Rittel, D. and Rabin, Y. (2000). "An investigation of the heat generated during cyclic loading of
530 two glassy polymers. part ii: Thermal analysis." *Mechanics of Materials*, 32(3), 149–159.

531 Rosakis, P., Rosakis, A., Ravichandran, G., and Hodowany, J. (2000). "A thermodynamic internal

variable model for the partition of plastic work into heat and stored energy in metals." *Journal of the Mechanics and Physics of Solids*, 48(3), 581–607.

Ryan, H. (1994). "Ricker, Ormsby, Klander, Butterworth - a choice of wavelets." *Canadian Society of Exploration Geophysicists Recorder*, 19(7), 8–9.

Simo, J. C. and Wong, K. K. (1991). "Unconditionally stable algorithms for rigid body dynamics that exactly preserve energy and momentum." *International journal for numerical methods in engineering*, 31(1), 19–52.

Veveakis, E., Sulem, J., and Stefanou, I. (2012). "Modeling of fault gouges with Cosserat continuum mechanics: Influence of thermal pressurization and chemical decomposition as coseismic weakening mechanisms." *Journal of Structural Geology*, 38, 254–264.

Watanabe, K., Pisanò, F., and Jeremić, B. (2017). "A numerical investigation on discretization effects in seismic wave propagation analyses." *Engineering with Computers*, 33(3), 519–545.

Yang, H., Feng, Y., Wang, H., and Jeremić, B. (2018a). "Energy dissipation analysis for inelastic reinforced concrete and steel beam-columns." *Engineering Structures, in review*.

Yang, H., Sinha, S. K., Feng, Y., McCallen, D. B., and Jeremić, B. (2018b). "Energy dissipation analysis of elastic-plastic materials." *Computer Methods in Applied Mechanics and Engineering*, 331, 309–326.

List of Tables

TABLE 1. Model parameters of the linear elastic material.

Parameter	Unit	Material
`mass_density` (ρ)	kg/m^3	2650
`poisson_ratio` (ν)		0.3
`shear_wave_velocity` (v_s)	m/s	800
`elastic_modulus` (E)	MPa	4409.6

TABLE 2. Model parameters of the inelastic materials.

Parameter	Unit	Material		
		Soft	Medium	Hard
`mass_density` (ρ)	kg/m^3	1800	1800	1800
`elastic_modulus` (E)	MPa	748.8	748.8	748.8
`poisson_ratio` (ν)		0.3	0.3	0.3
`von_mises_radius`	MPa	1.0	1.0	1.0
`armstrong_frederick_ha` (h_a)	MPa	374.4	748.8	1497.6
`armstrong_frederick_cr` (c_r)		50	100	200

TABLE 3. Rayleigh damping parameters for the single element examples using linear elastic material with Rayleigh damping.

Parameter	Unit	Case 1	Case 2	Case 3	Case 4
R		5.0	5.0	5.0	5.0
T_1	s	1.0	1.0	1.0	1.0
ξ		0.02	0.05	0.10	0.20

TABLE 4. Rayleigh damping parameters for the wave propagation examples using linear elastic material with Rayleigh damping.

Parameter	Unit	Case 1	Case 2	Case 3
R		5.0	5.0	5.0
T_1	s	1.0	1.0	1.0
ξ		0.02	0.05	0.10

List of Figures

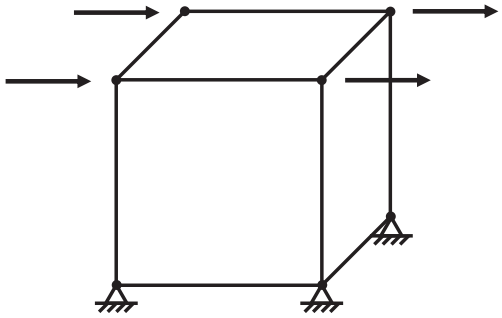

Fig. 1. Single element model under shear loading.

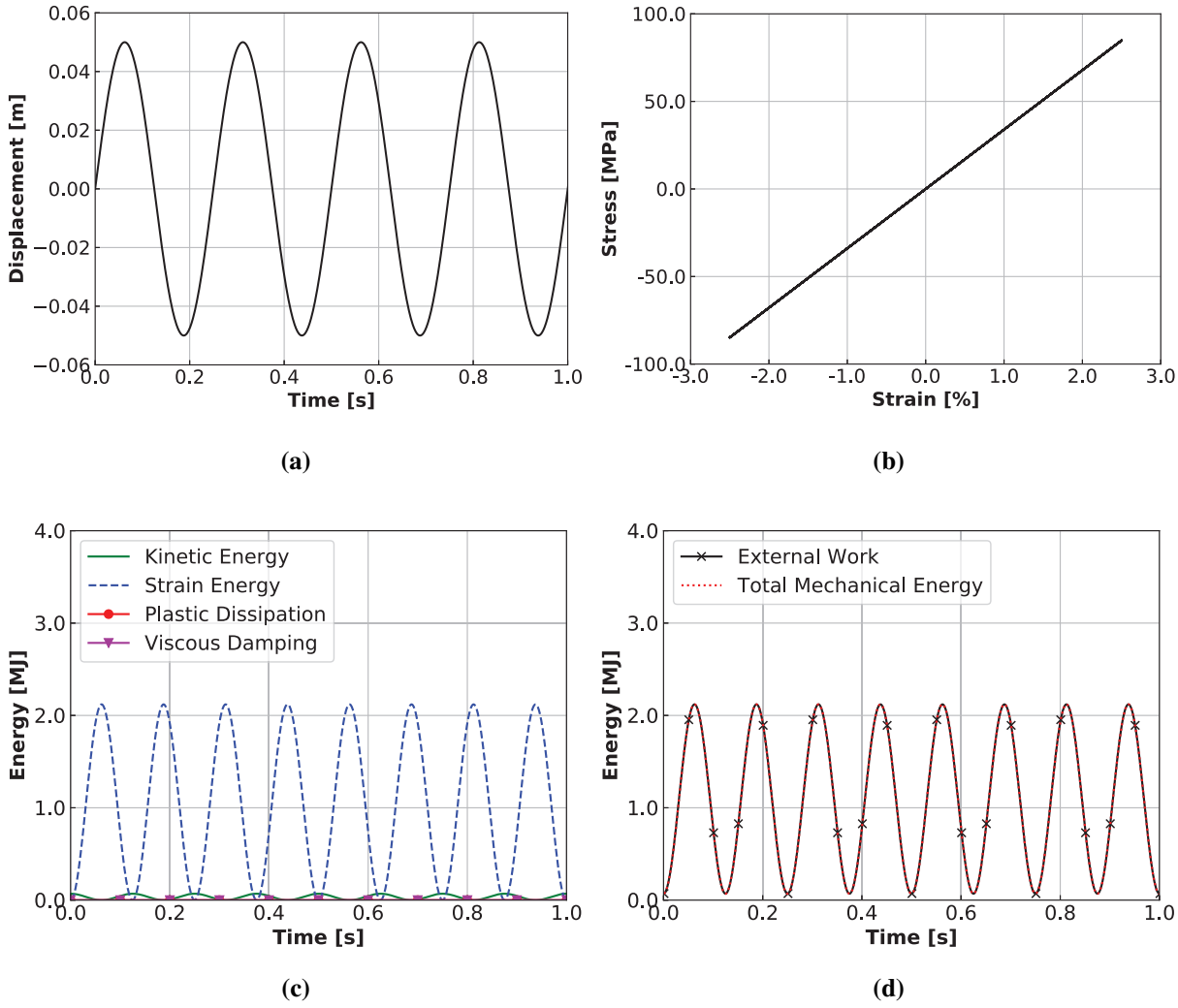

Fig. 2. Energy computation of single brick element modeled using linear elastic material and no Rayleigh damping: (a) Displacement time series; (b) Stress-strain response; (c) Energy results; (d) External work.

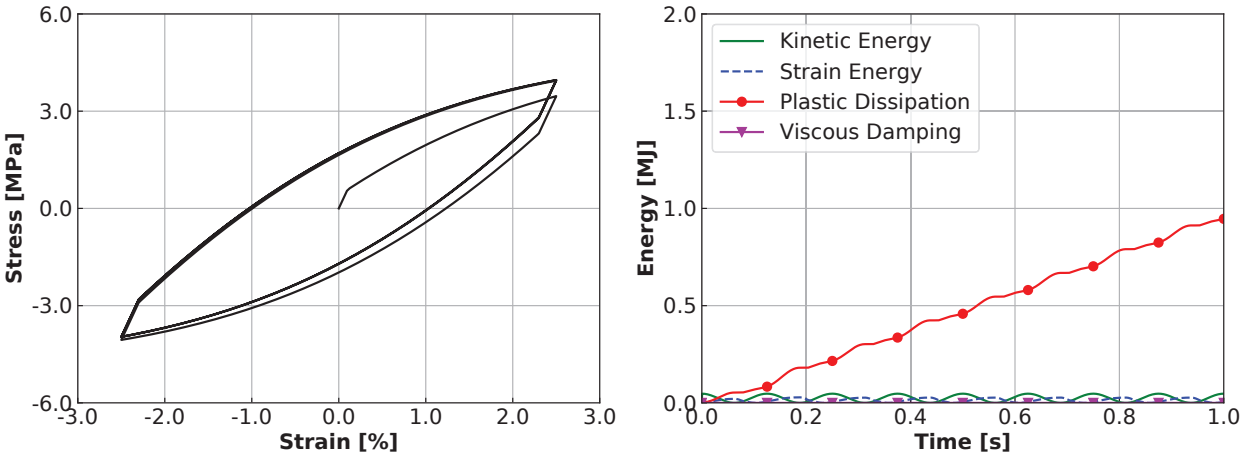

(a)

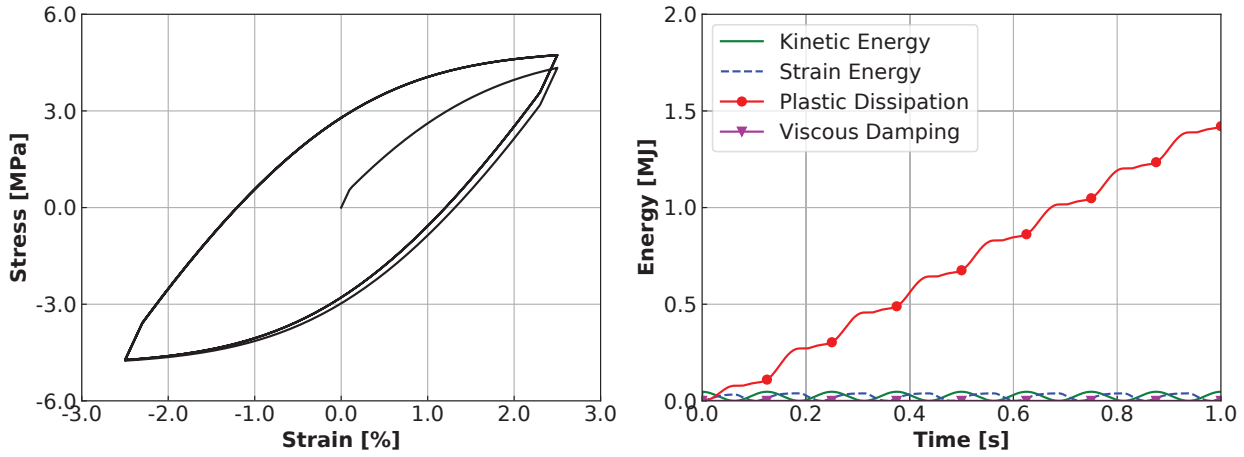

(b)

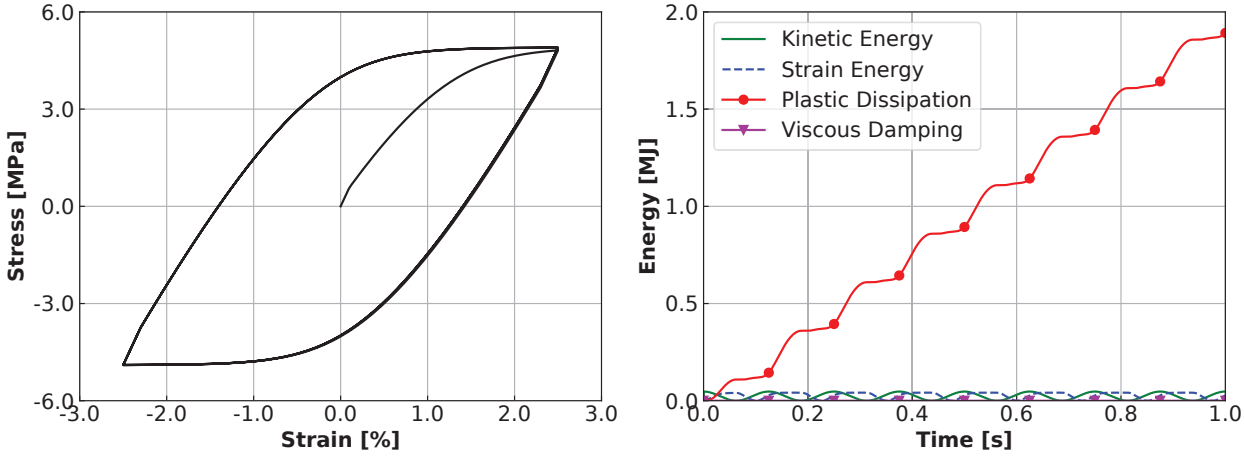

(c)

Fig. 3. Energy computation for a single brick element modeled using inelastic material and no Rayleigh damping: (a) Soft material; (b) Medium material; (c) Hard material.

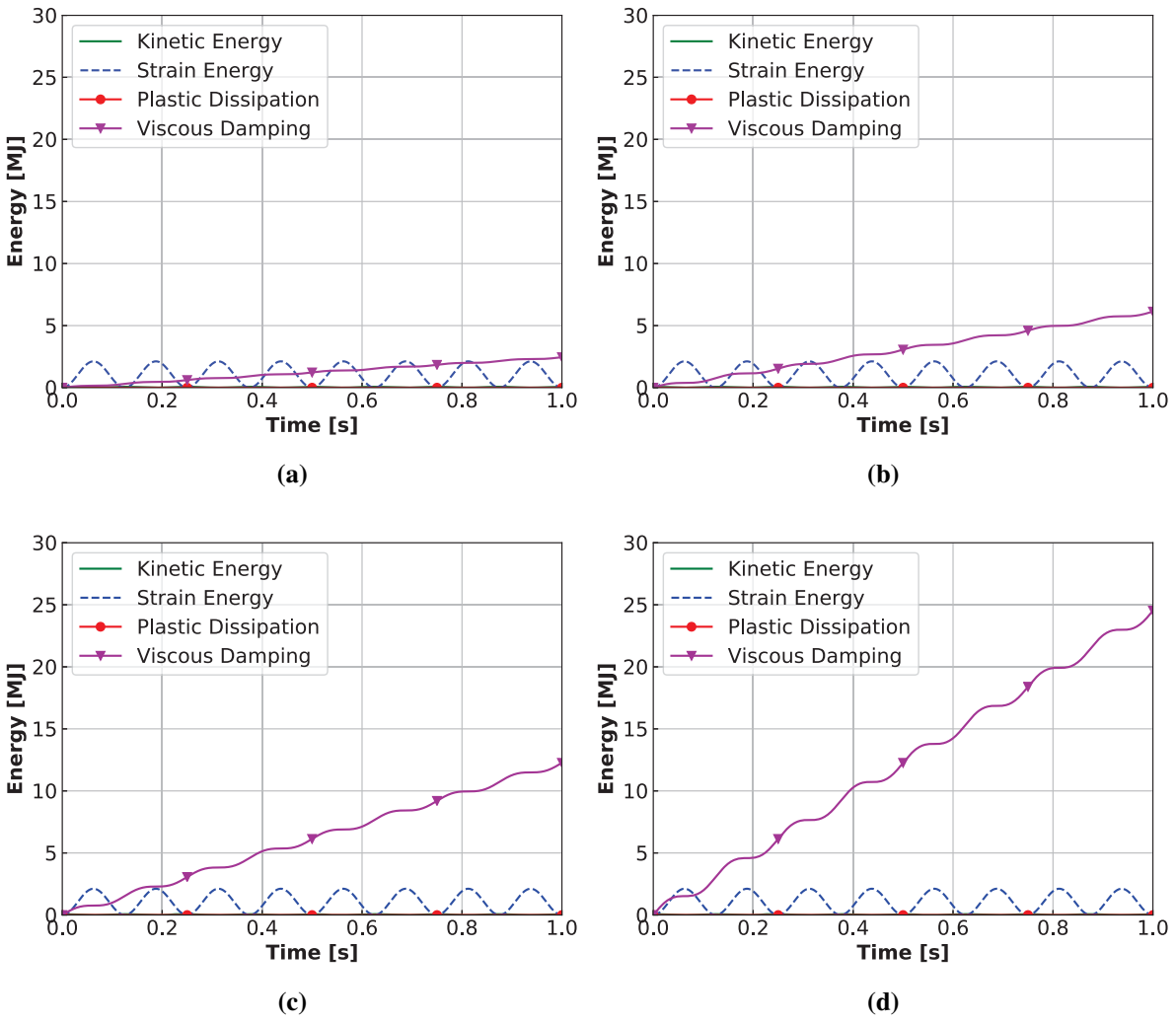

Fig. 4. Energy computation of single brick element modeled using elastic material with Rayleigh damping: (a) $\xi = 0.02$; (b) $\xi = 0.05$; (c) $\xi = 0.10$; (d) $\xi = 0.20$.

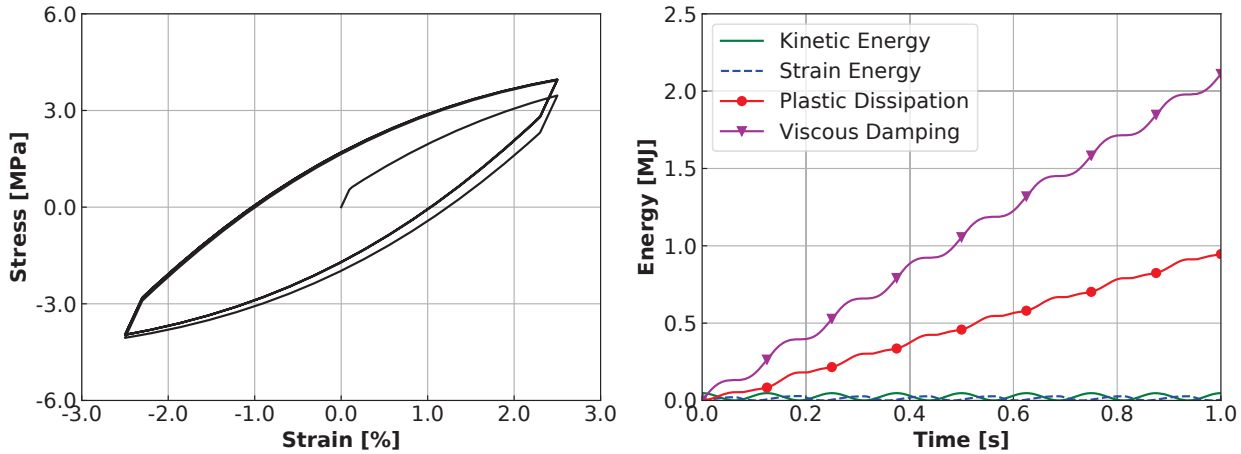

(a)

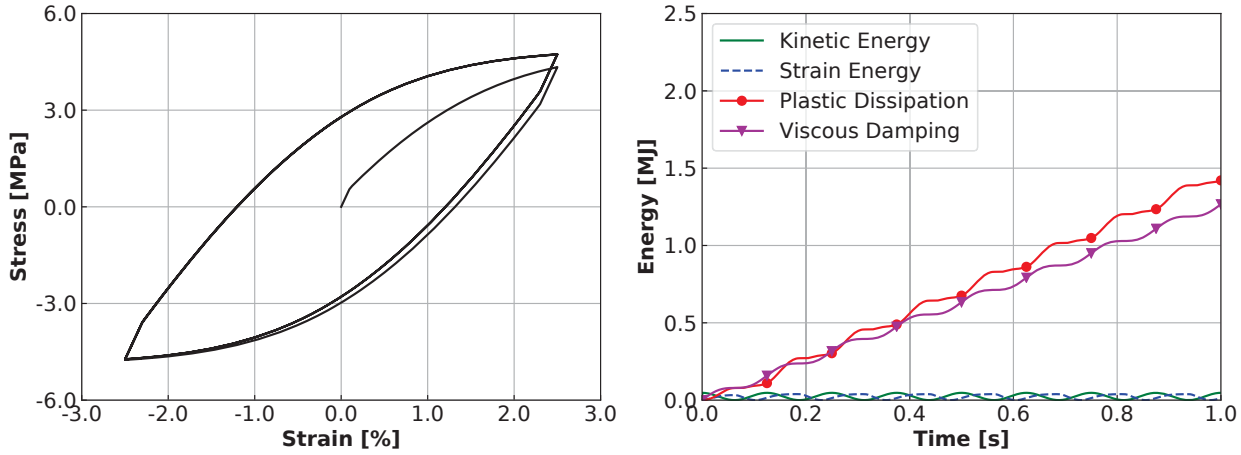

(b)

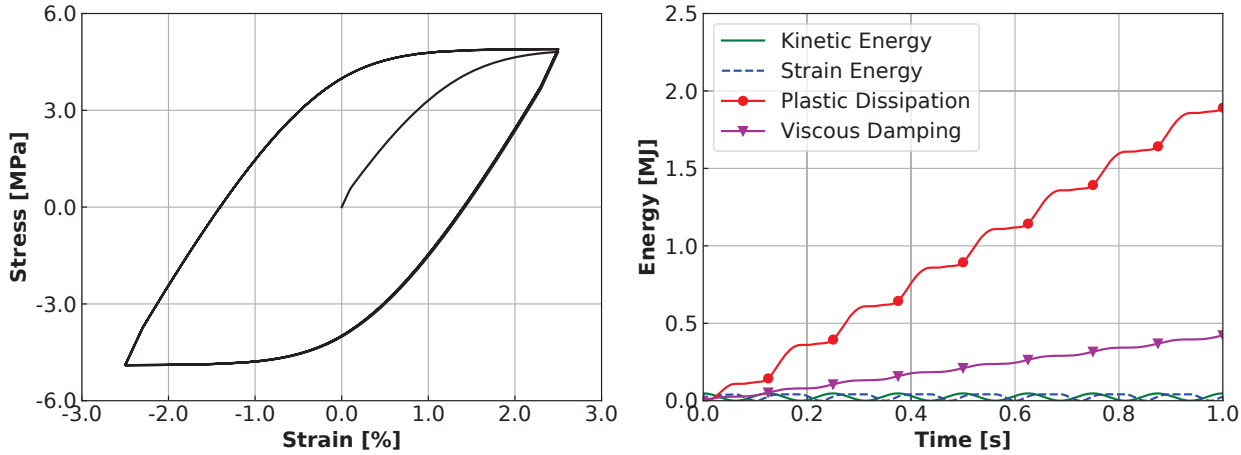

(c)

Fig. 5. Energy computation of single brick element modeled using inelastic material with Rayleigh damping: (a) Soft material, $\xi = 0.1$; (b) Medium material, $\xi = 0.06$; (c) Hard material, $\xi = 0.02$.

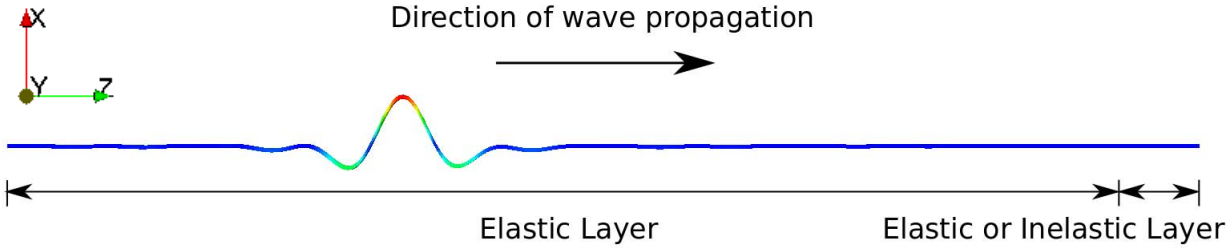

Fig. 6. Numerical model of the wave propagation problem used in this paper.

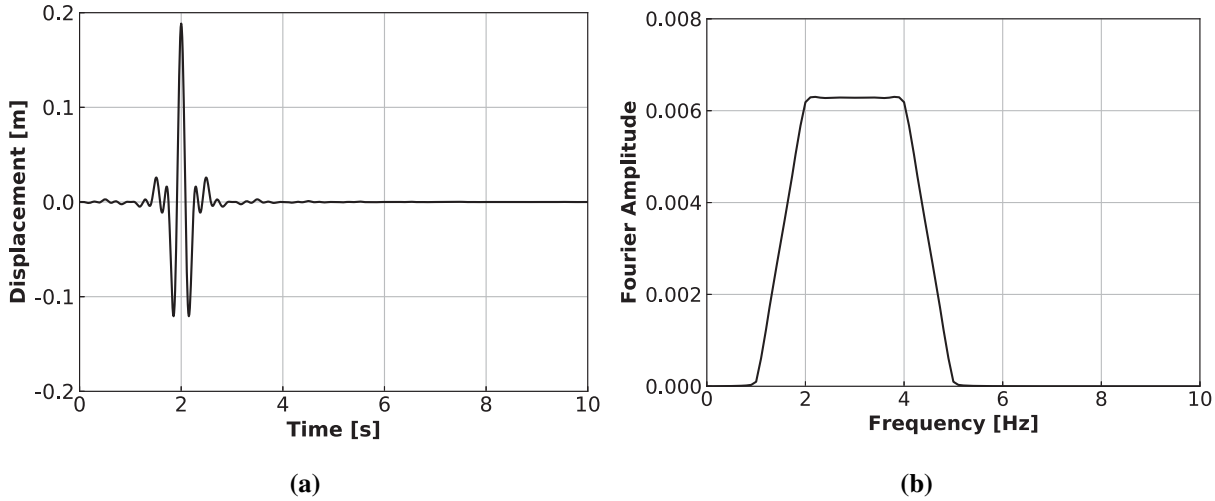

Fig. 7. Imposed displacement of the wave propagation problem created using Ormsby wavelet with $A = 0.01\text{m}\cdot\text{s}$, $f_1 = 1.0\text{Hz}$, $f_2 = 2.0\text{Hz}$, $f_3 = 4.0\text{Hz}$, and $f_4 = 5.0\text{Hz}$: (a) Time series; (b) Frequency domain.

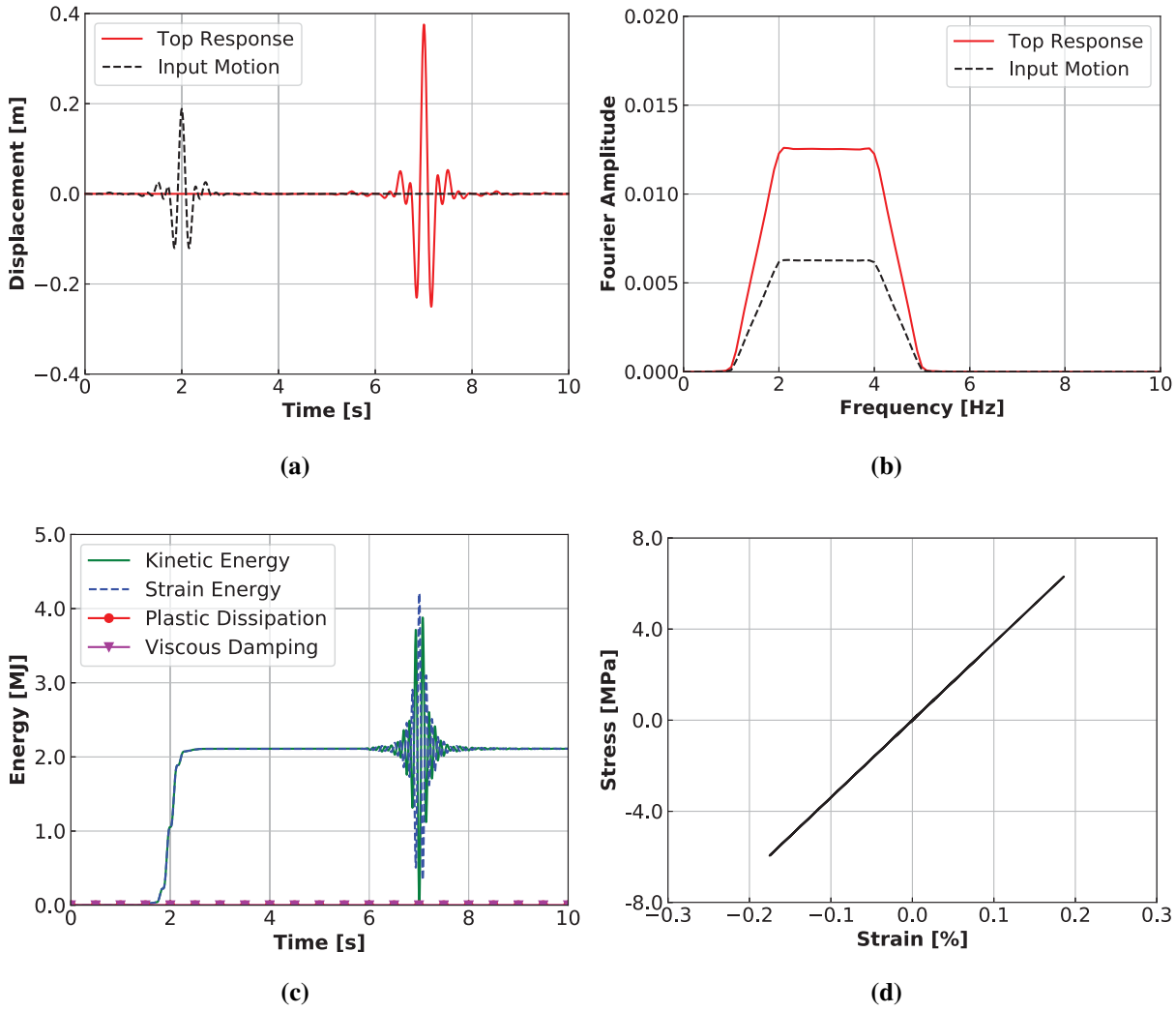

Fig. 8. Energy computation of wave propagation within an uniform elastic media: (a) Displacement time series; (b) Displacement spectrum; (c) Energy results; (d) Stress-strain response.

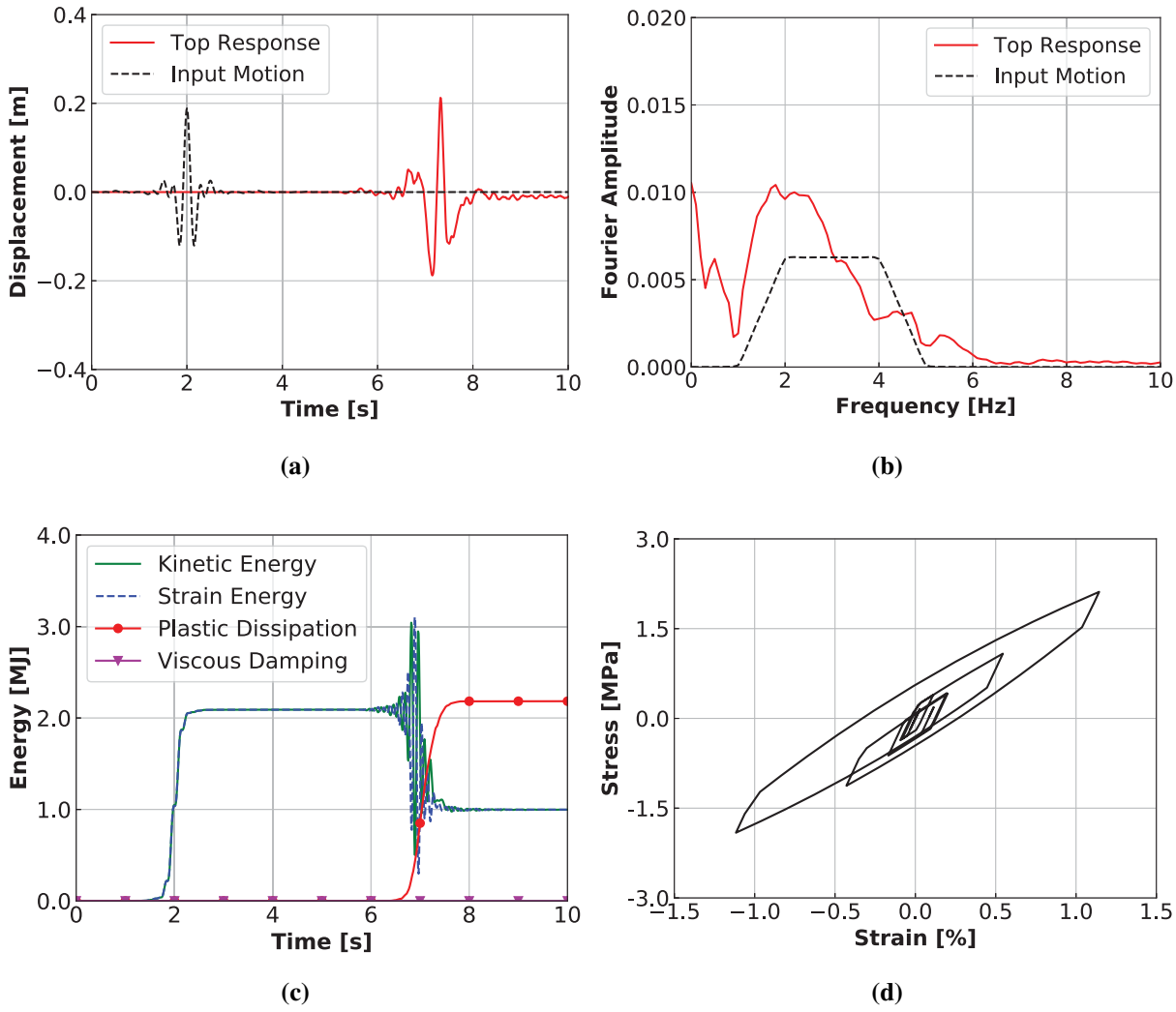

Fig. 9. Energy computation of wave propagation using soft inelastic material and no Rayleigh damping: (a) Displacement time series; (b) Displacement spectrum; (c) Energy results; (d) Stress-strain response.

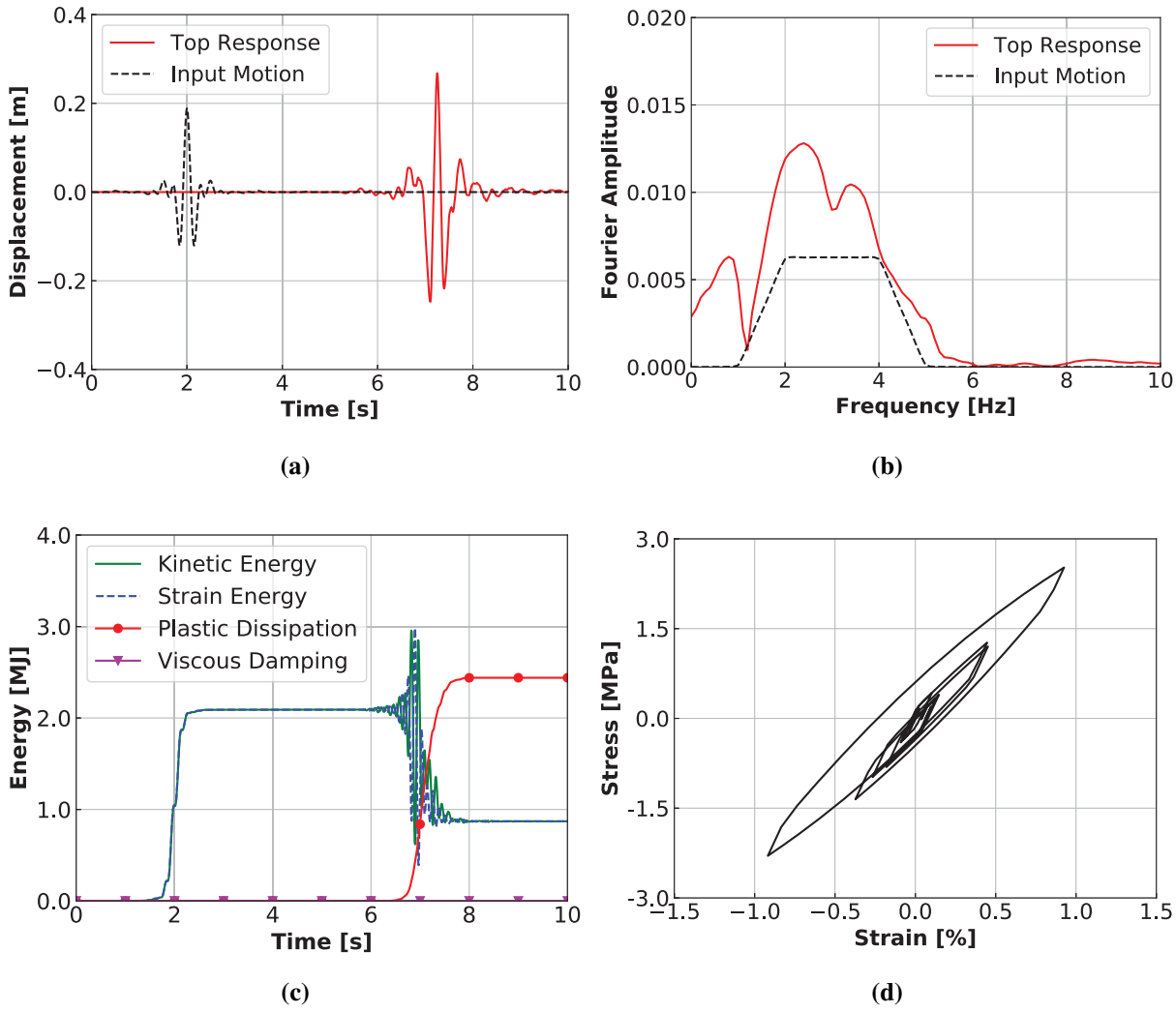

Fig. 10. Energy computation of wave propagation using medium inelastic material and no Rayleigh damping: (a) Displacement time series; (b) Displacement spectrum; (c) Energy results; (d) Stress-strain response.

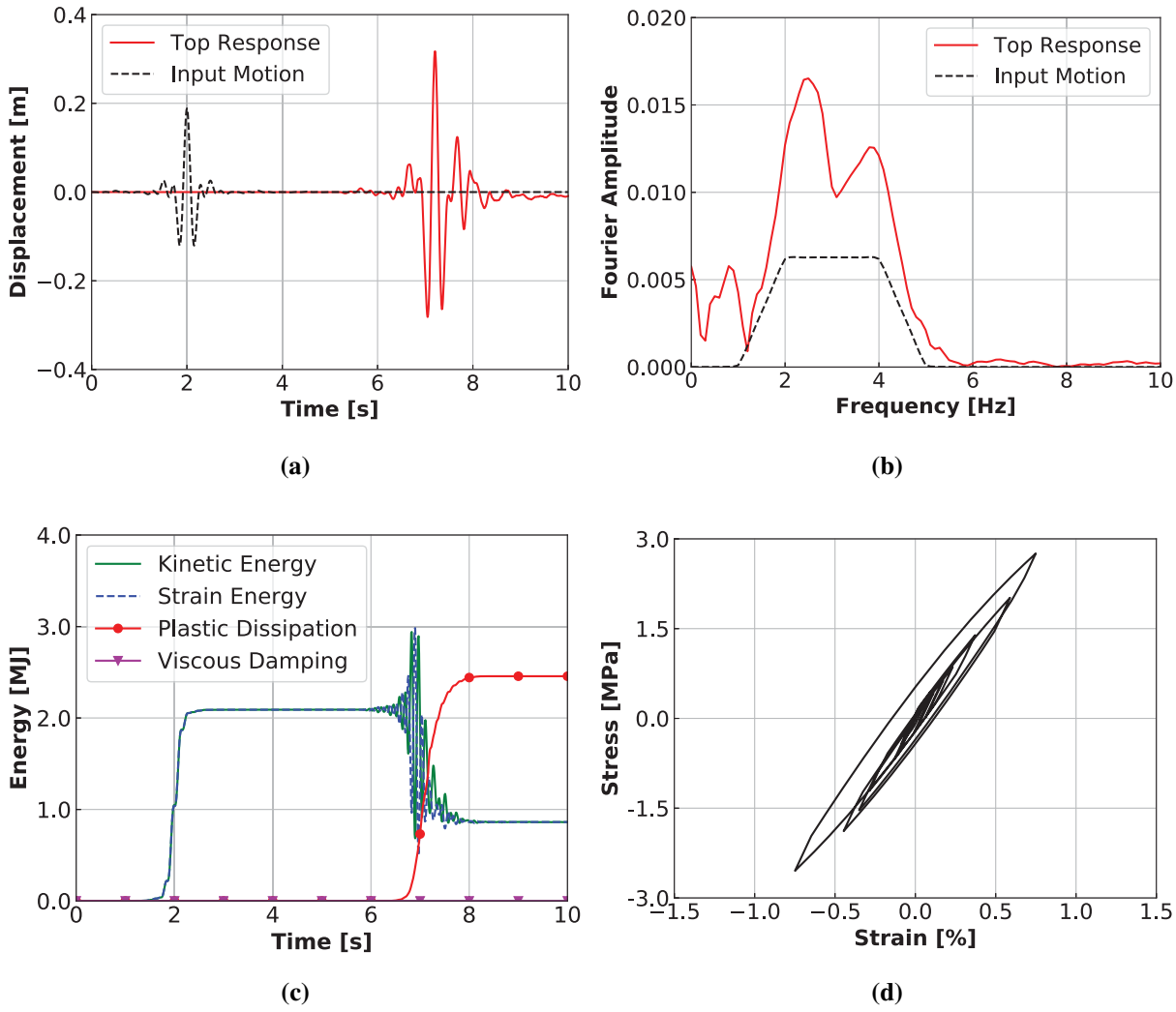

Fig. 11. Energy computation of wave propagation using hard inelastic material and no Rayleigh damping: (a) Displacement time series; (b) Displacement spectrum; (c) Energy results; (d) Stress-strain response.

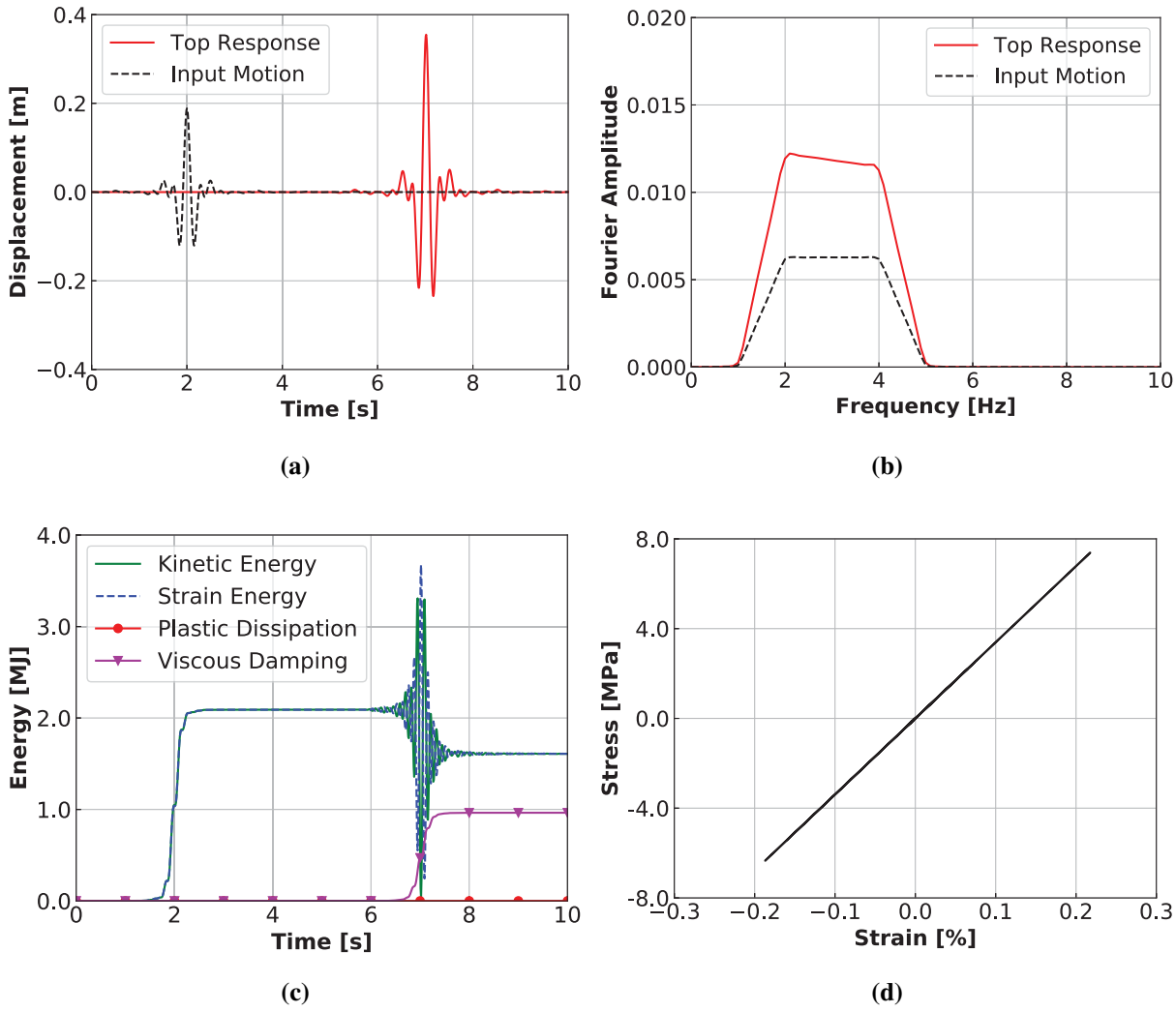

Fig. 12. Energy computation of wave propagation using linear elastic material and Rayleigh damping ($\xi = 0.02$): (a) Displacement time series; (b) Displacement spectrum; (c) Energy results; (d) Stress-strain response.

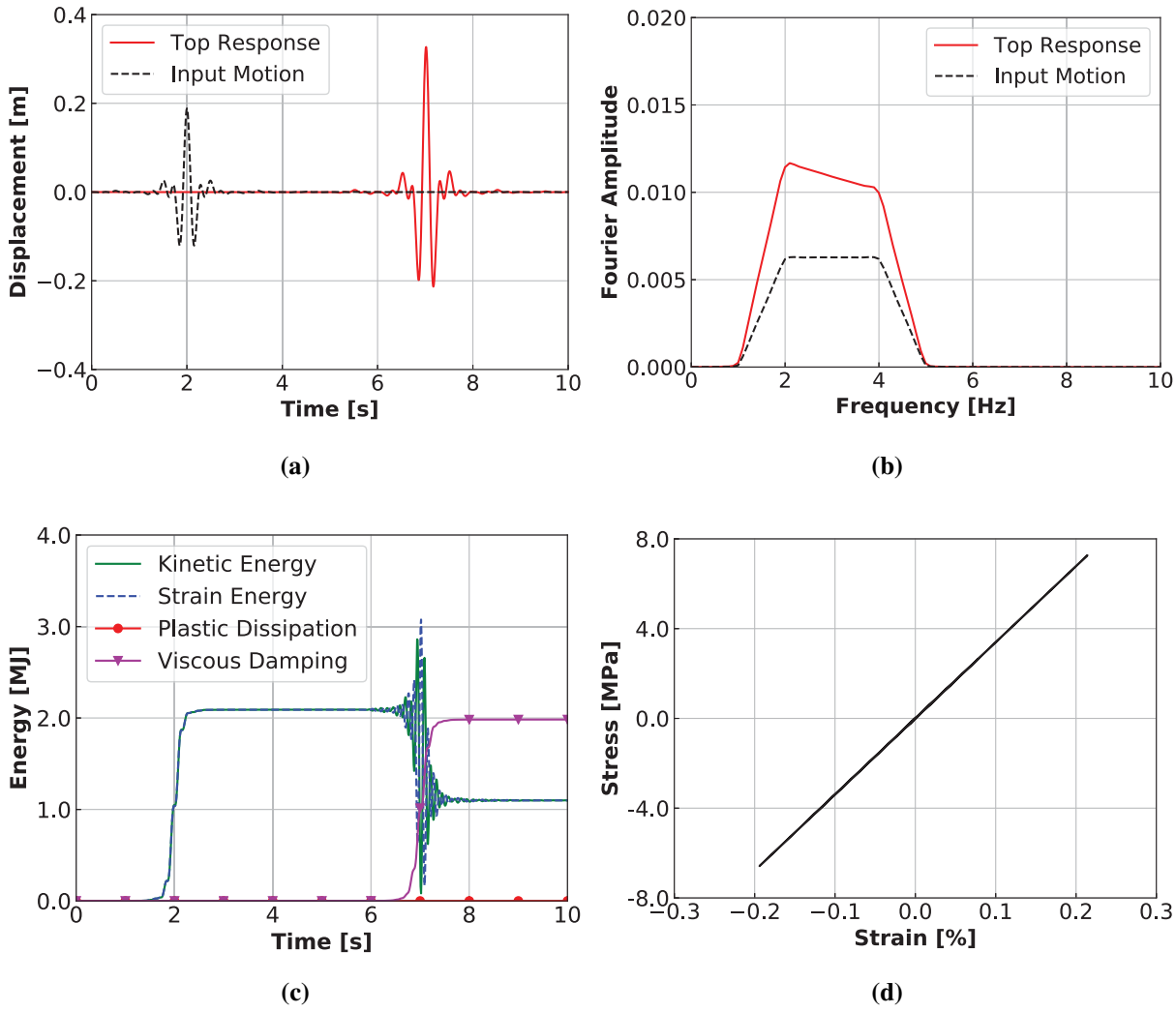

Fig. 13. Energy computation of wave propagation using linear elastic material and Rayleigh damping ($\xi = 0.05$): (a) Displacement time series; (b) Displacement spectrum; (c) Energy results; (d) Stress-strain response.

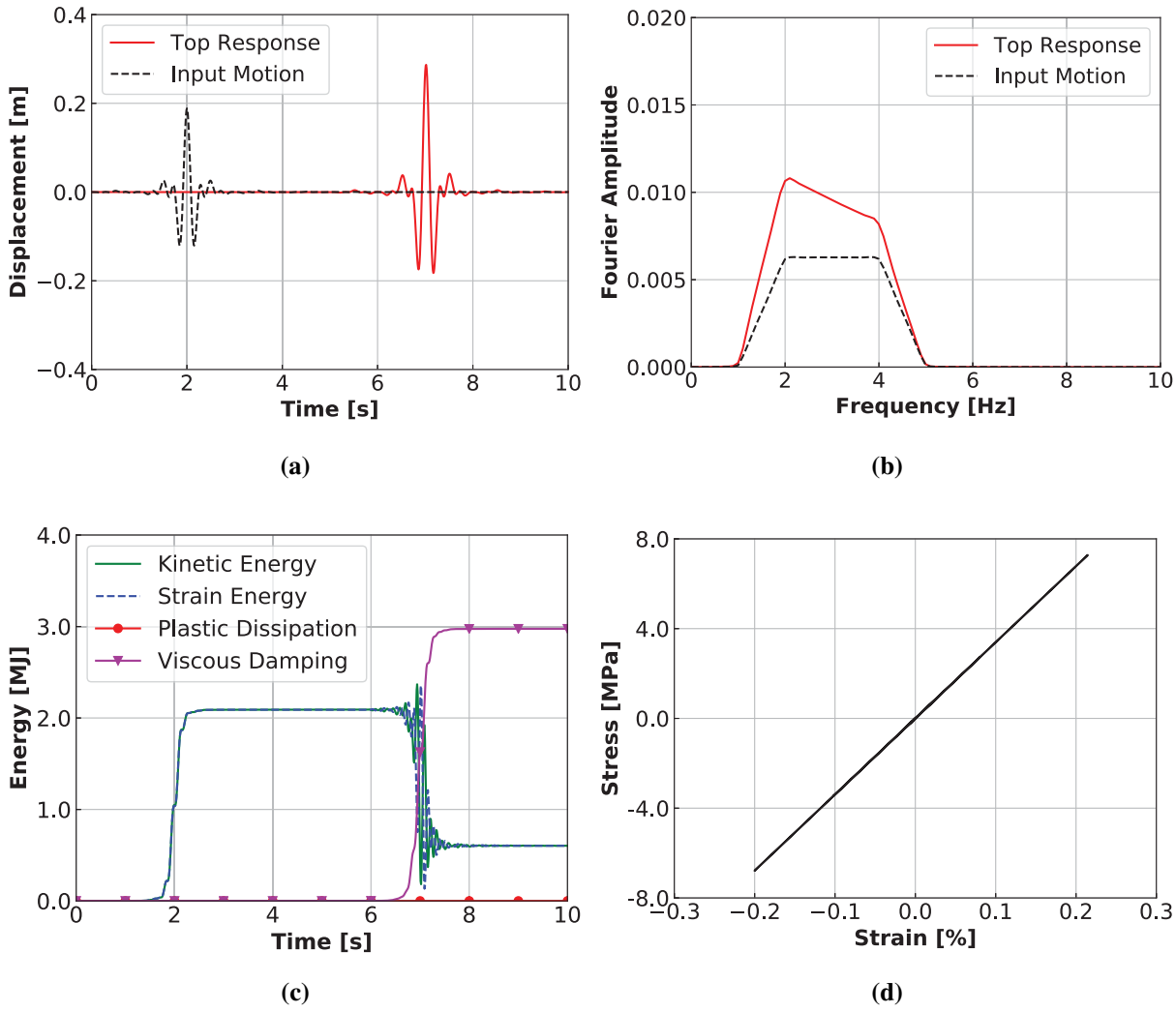

Fig. 14. Energy computation of wave propagation using linear elastic material and Rayleigh damping ($\xi = 0.10$): (a) Displacement time series; (b) Displacement spectrum; (c) Energy results; (d) Stress-strain response.

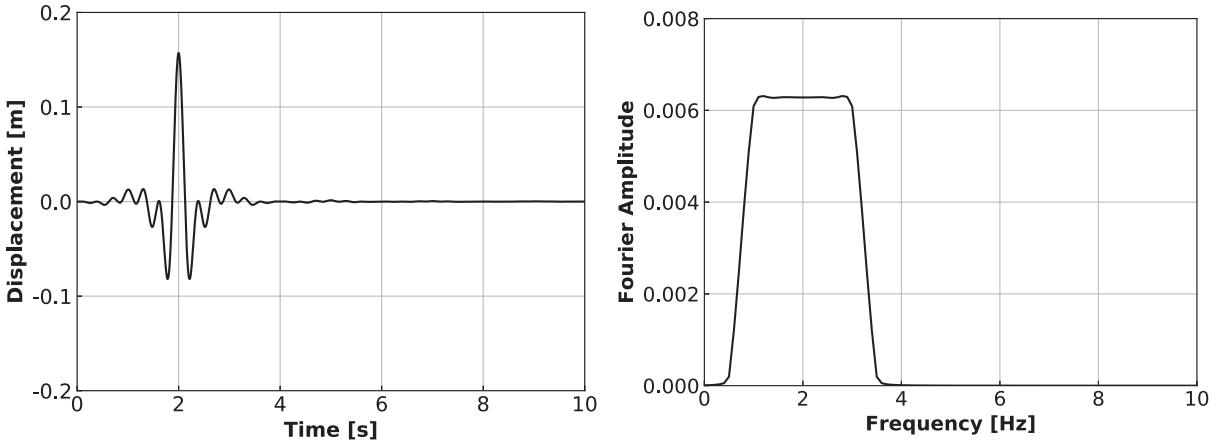

(a) **(b)**

Fig. 15. Imposed displacement of the wave propagation problem created using Ormsby wavelet with $A = 0.01$m·s, $f_1 = 0.5$Hz, $f_2 = 1.0$Hz, $f_3 = 3.0$Hz, and $f_4 = 3.5$Hz: (a) Time series; (b) Frequency domain.

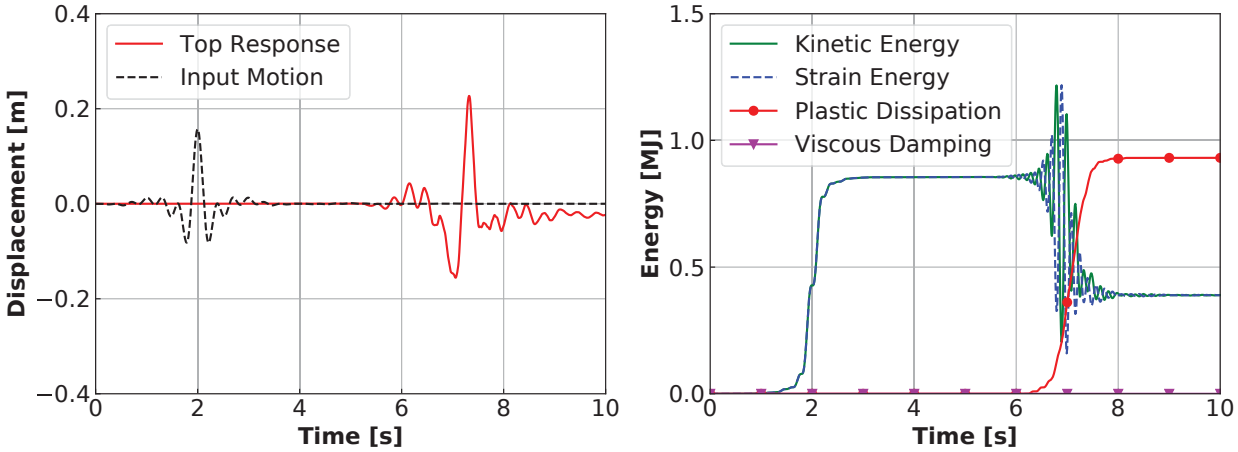

(a)

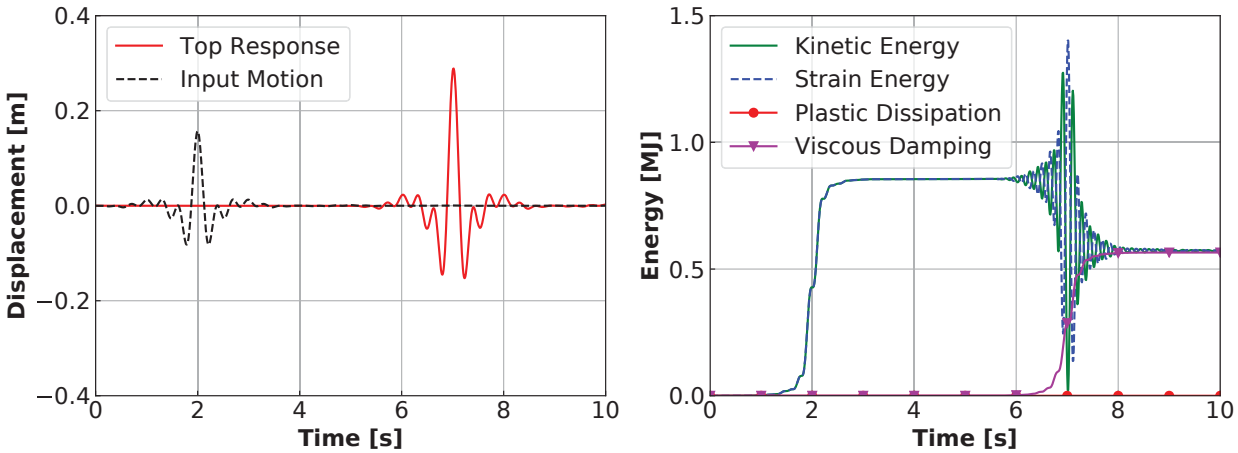

(b)

Fig. 16. Energy computation of wave propagation using a different input motion: (a) Soft inelastic material without Rayleigh damping; (b) Linear elastic material with Rayleigh damping $\xi = 0.05$.

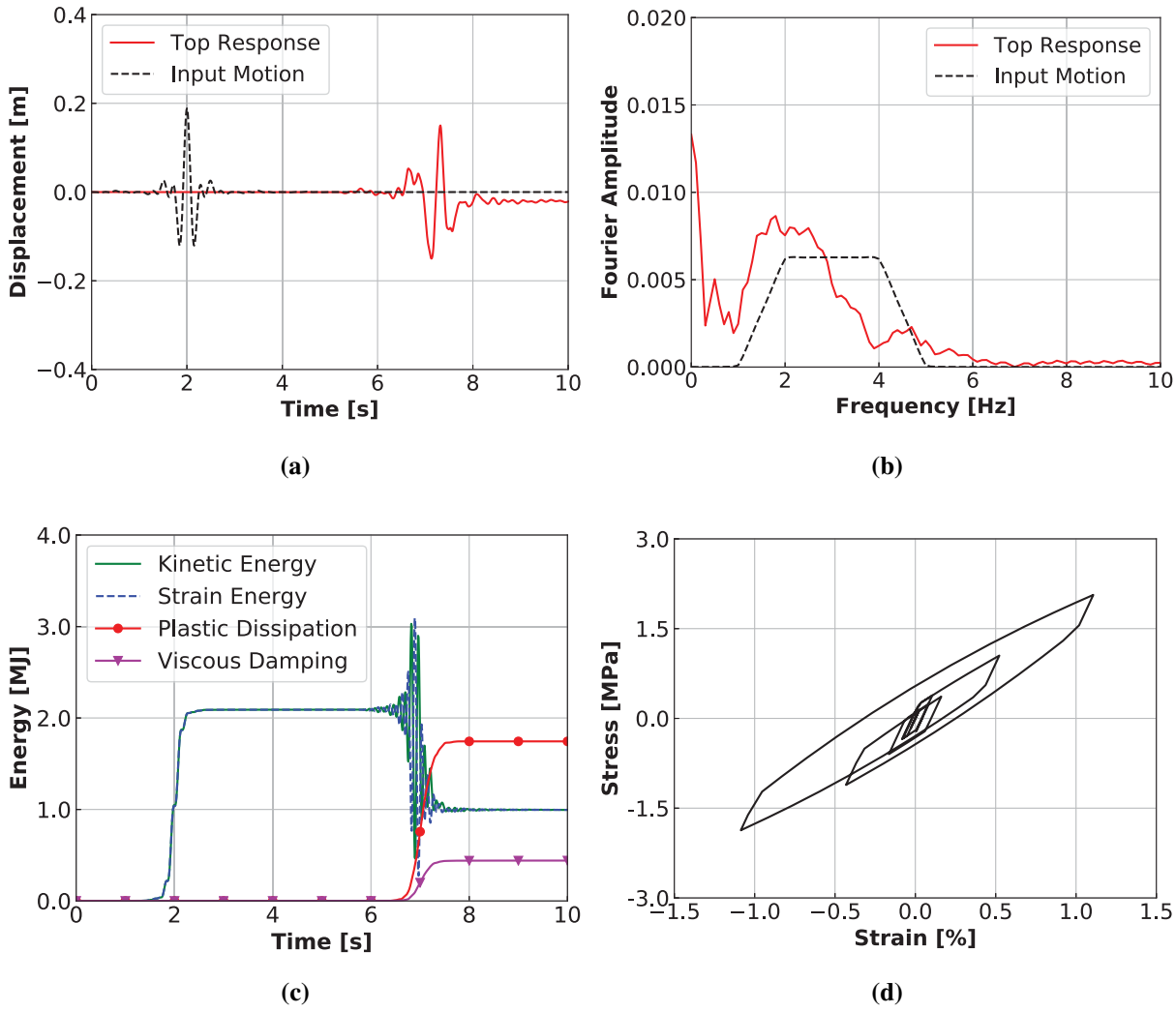

Fig. 17. Energy computation of wave propagation using soft inelastic material and Rayleigh damping with $\xi = 0.01$: (a) Displacement time series; (b) Displacement spectrum; (c) Energy results; (d) Stress-strain response.

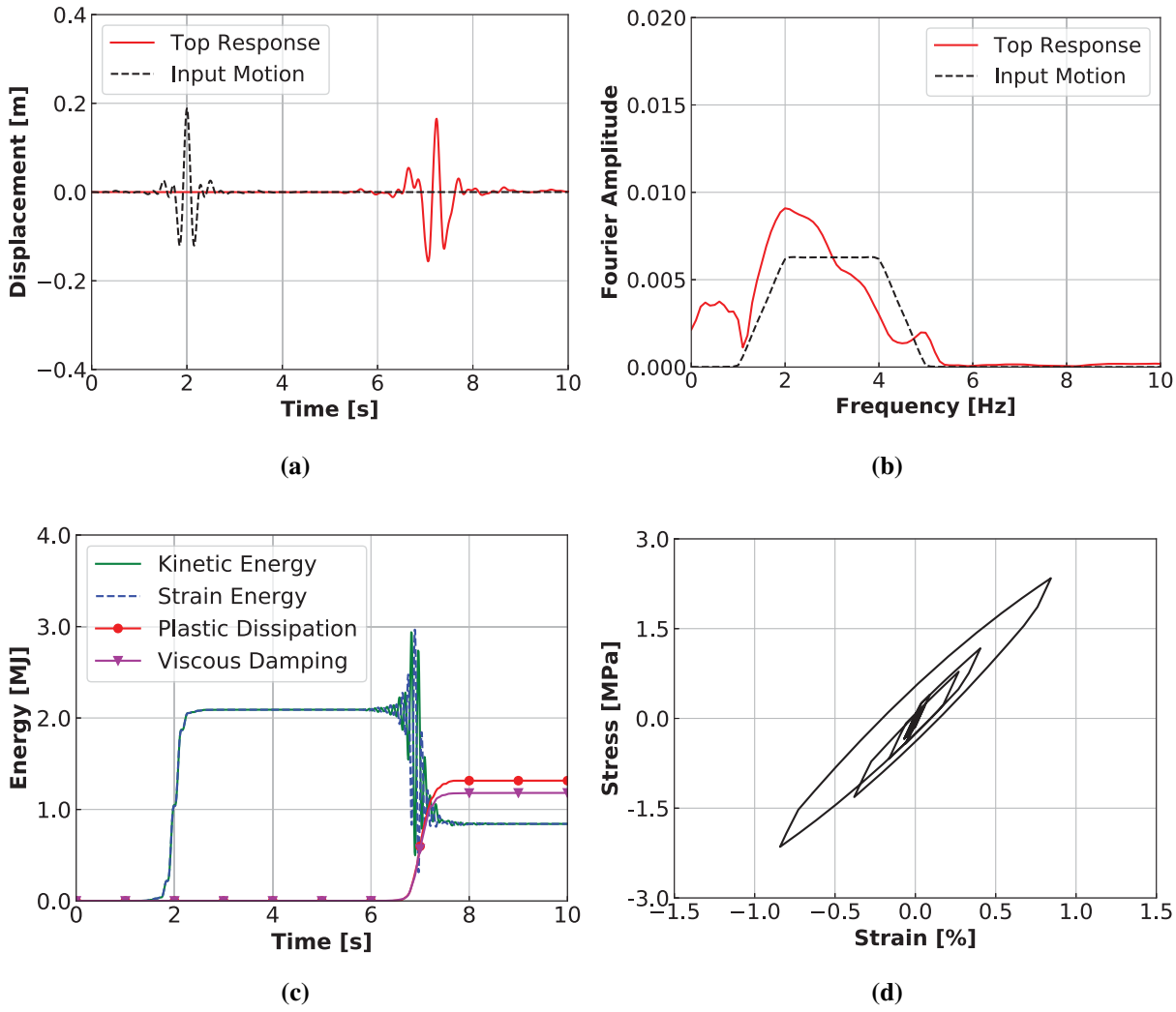

Fig. 18. Energy computation of wave propagation using medium inelastic material model and Rayleigh damping with $\xi = 0.04$: (a) Displacement time series; (b) Displacement spectrum; (c) Energy results; (d) Stress-strain response.

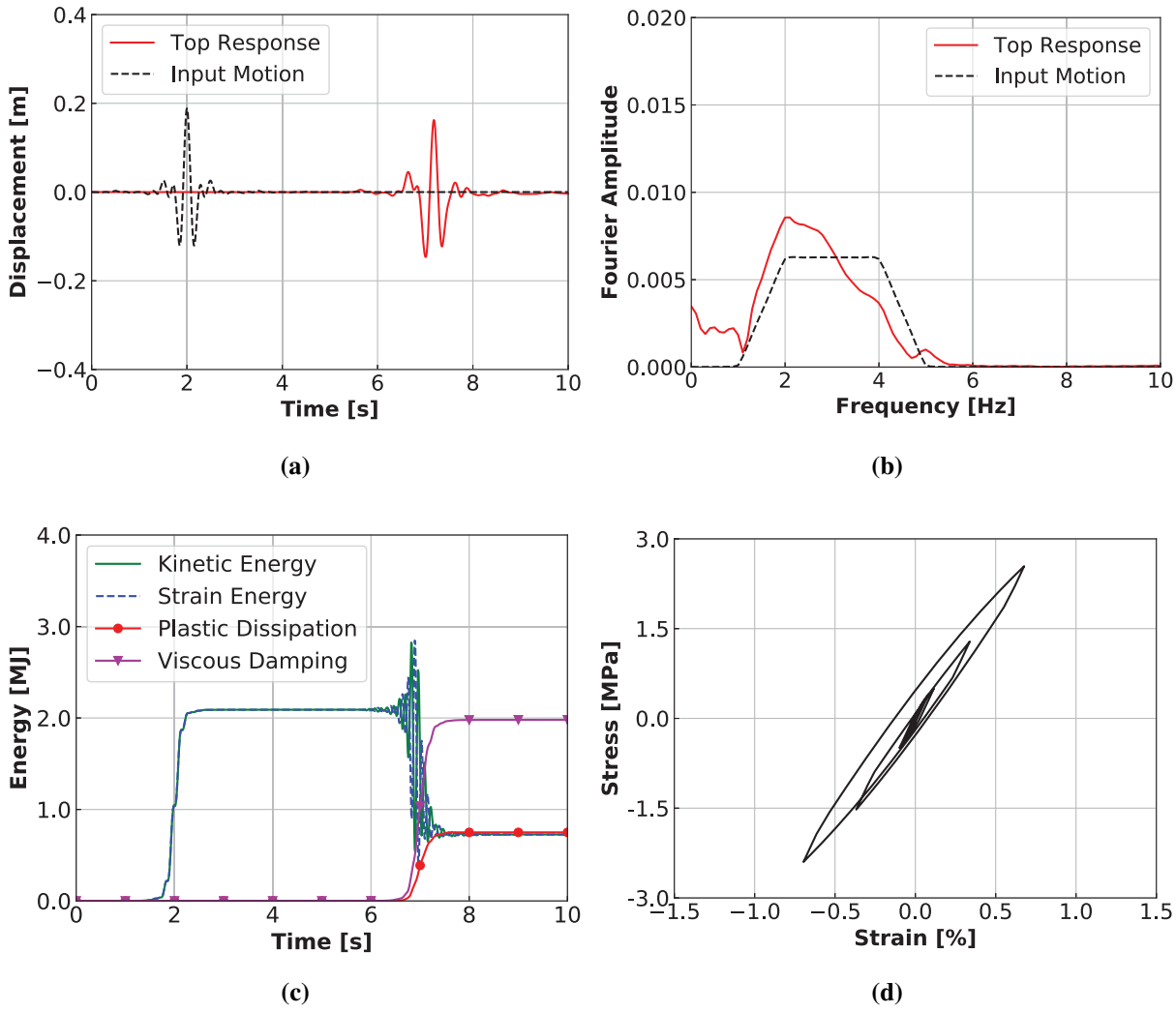

Fig. 19. Energy computation of wave propagation using hard inelastic material model and Rayleigh damping with $\xi = 0.10$: (a) Displacement time series; (b) Displacement spectrum; (c) Energy results; (d) Stress-strain response.

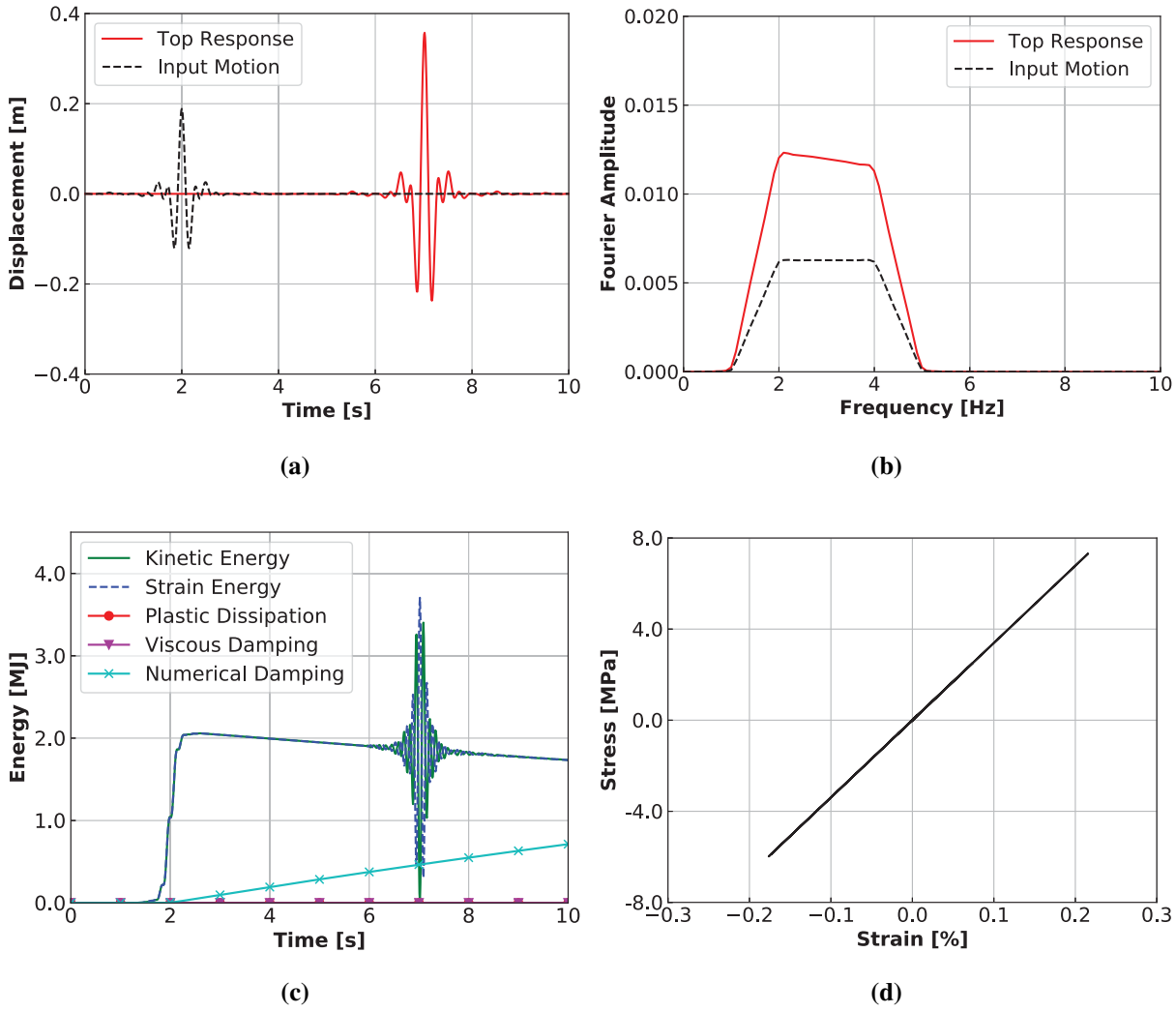

Fig. 20. Energy computation of wave propagation using linear elastic material and algorithmic damping ($\gamma = 0.505$, $\beta = 0.253$): (a) Displacement time series; (b) Displacement spectrum; (c) Energy results; (d) Stress-strain response.

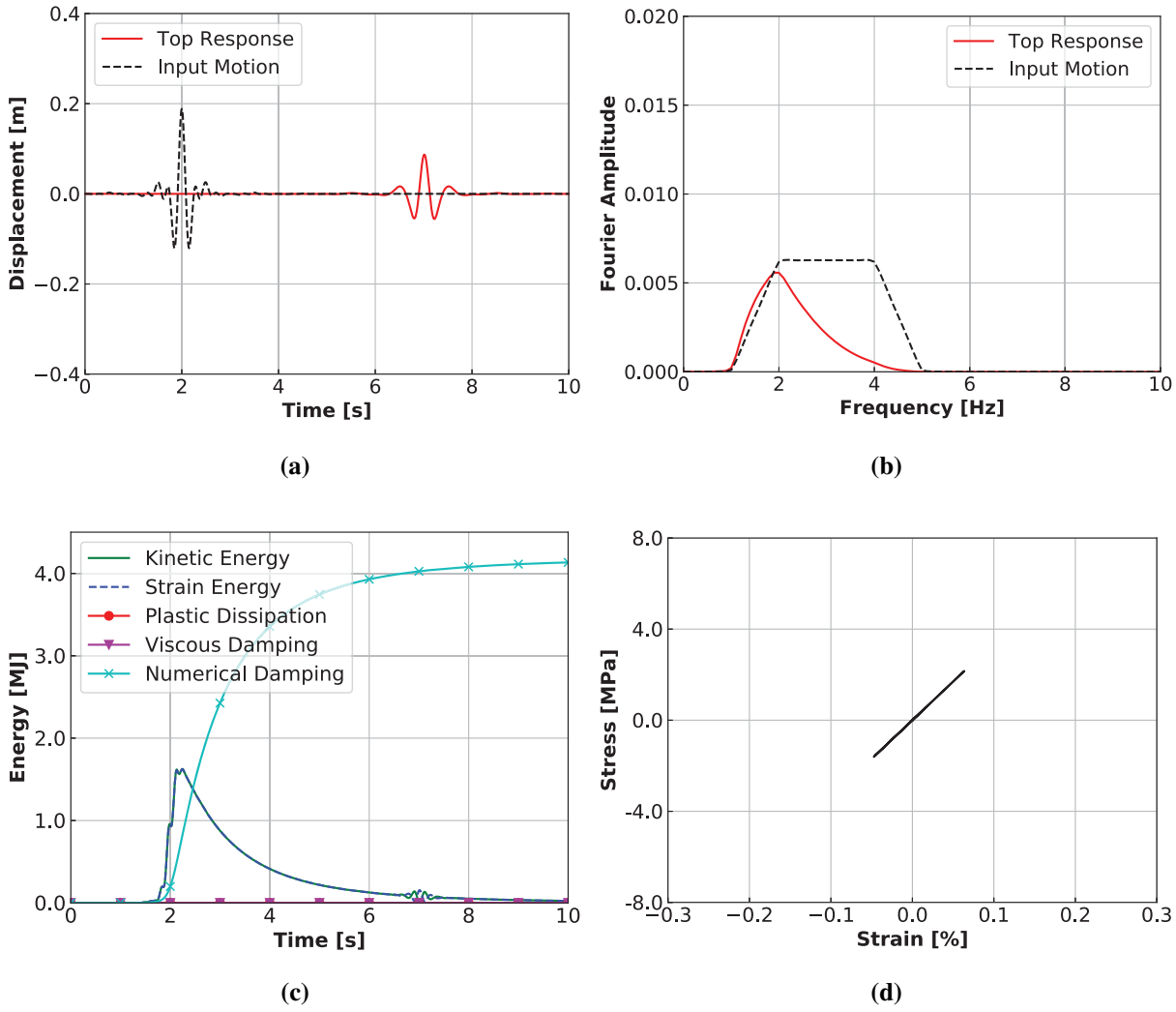

Fig. 21. Energy computation of wave propagation using linear elastic material model and algorithmic damping ($\gamma = 0.700$, $\beta = 0.360$): (a) Displacement time series; (b) Displacement spectrum; (c) Energy results; (d) Stress-strain response.

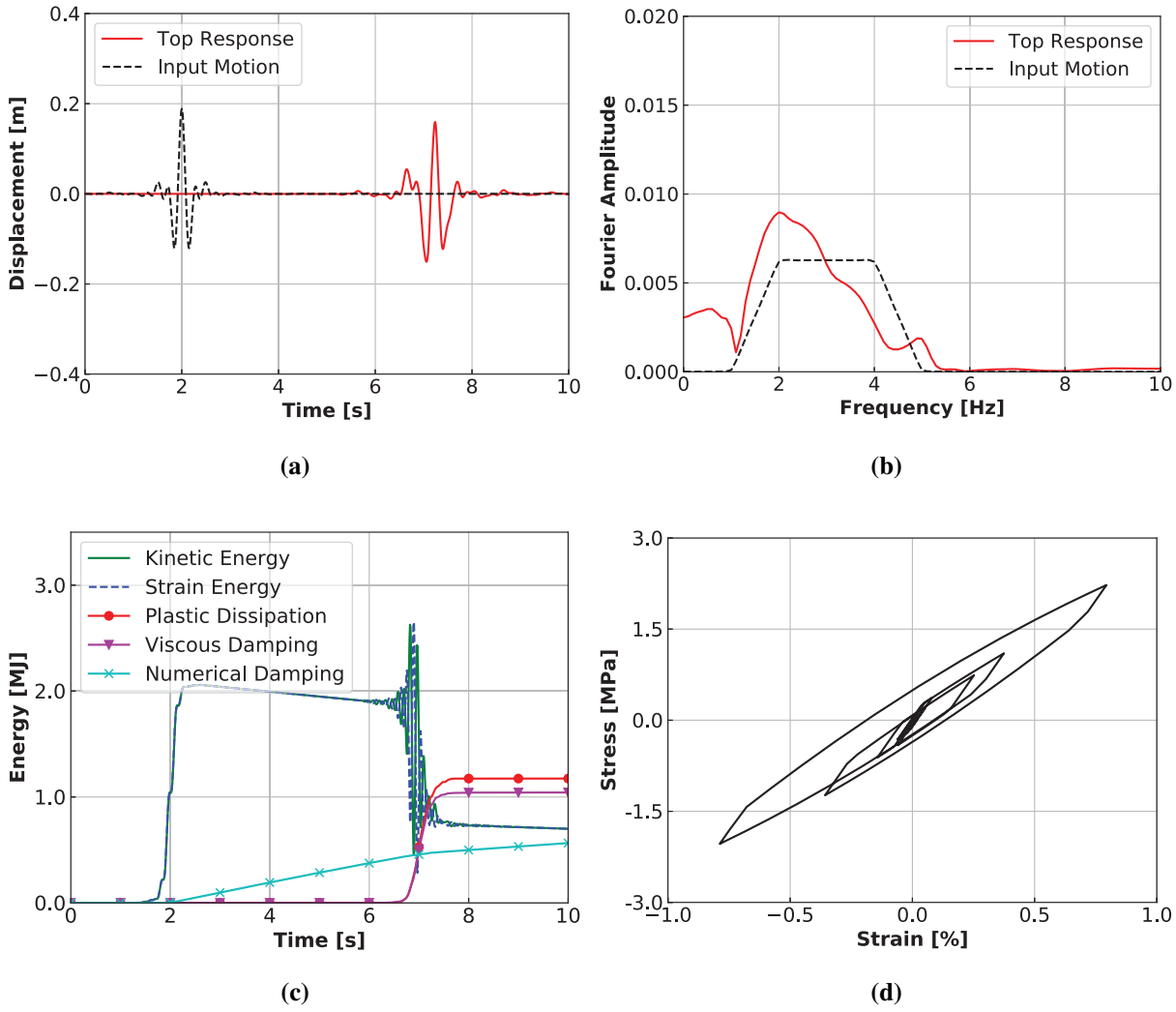

Fig. 22. Energy computation of wave propagation using medium inelastic material model, Rayleigh damping ($\xi = 0.04$), and algorithmic damping ($\gamma = 0.505$, $\beta = 0.253$): (a) Displacement time series; (b) Displacement spectrum; (c) Energy results; (d) Stress-strain response.

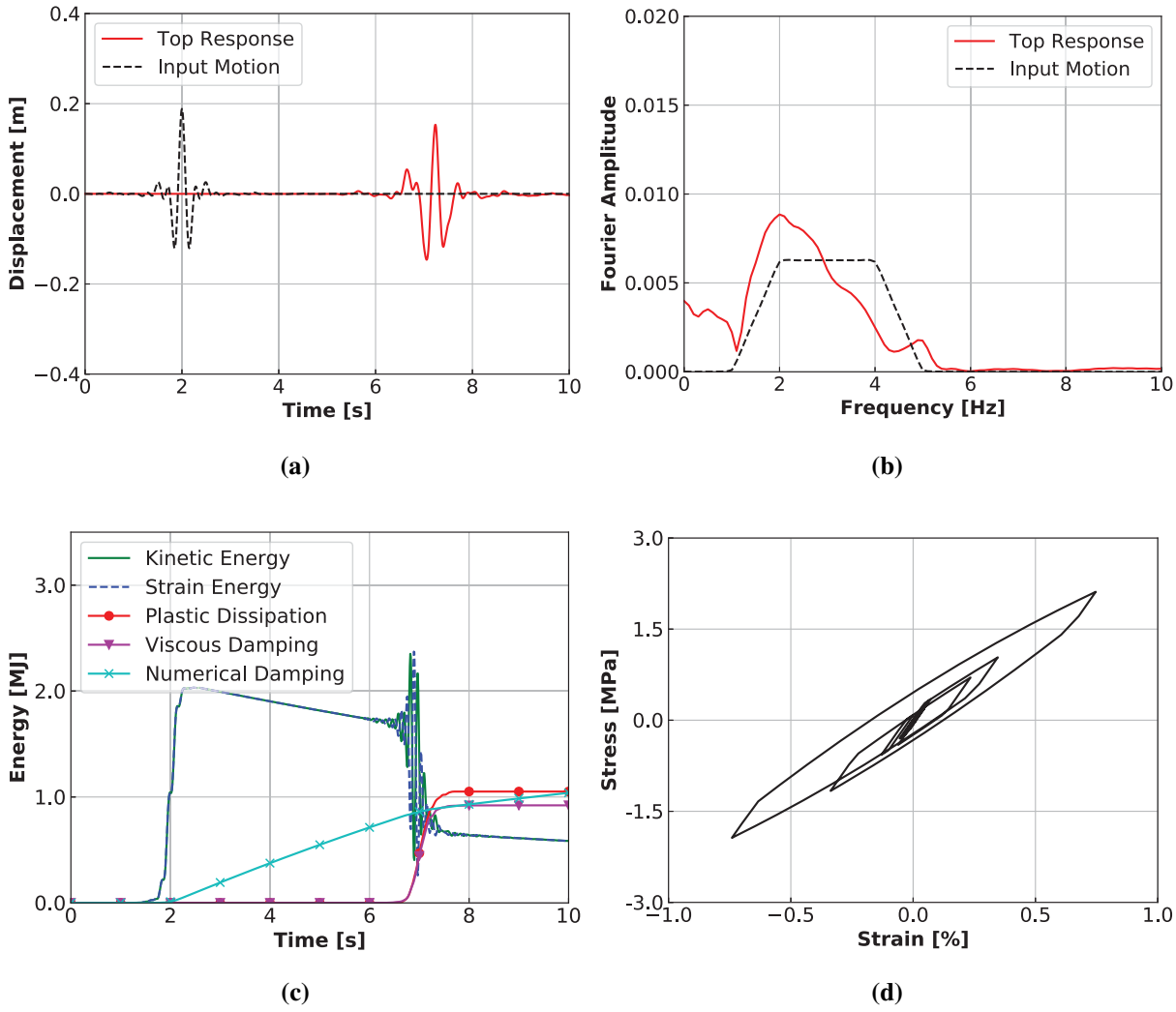

Fig. 23. Energy computation of wave propagation using medium inelastic material model, Rayleigh damping ($\xi = 0.04$), and algorithmic damping ($\gamma = 0.510$, $\beta = 0.255$): (a) Displacement time series; (b) Displacement spectrum; (c) Energy results; (d) Stress-strain response.

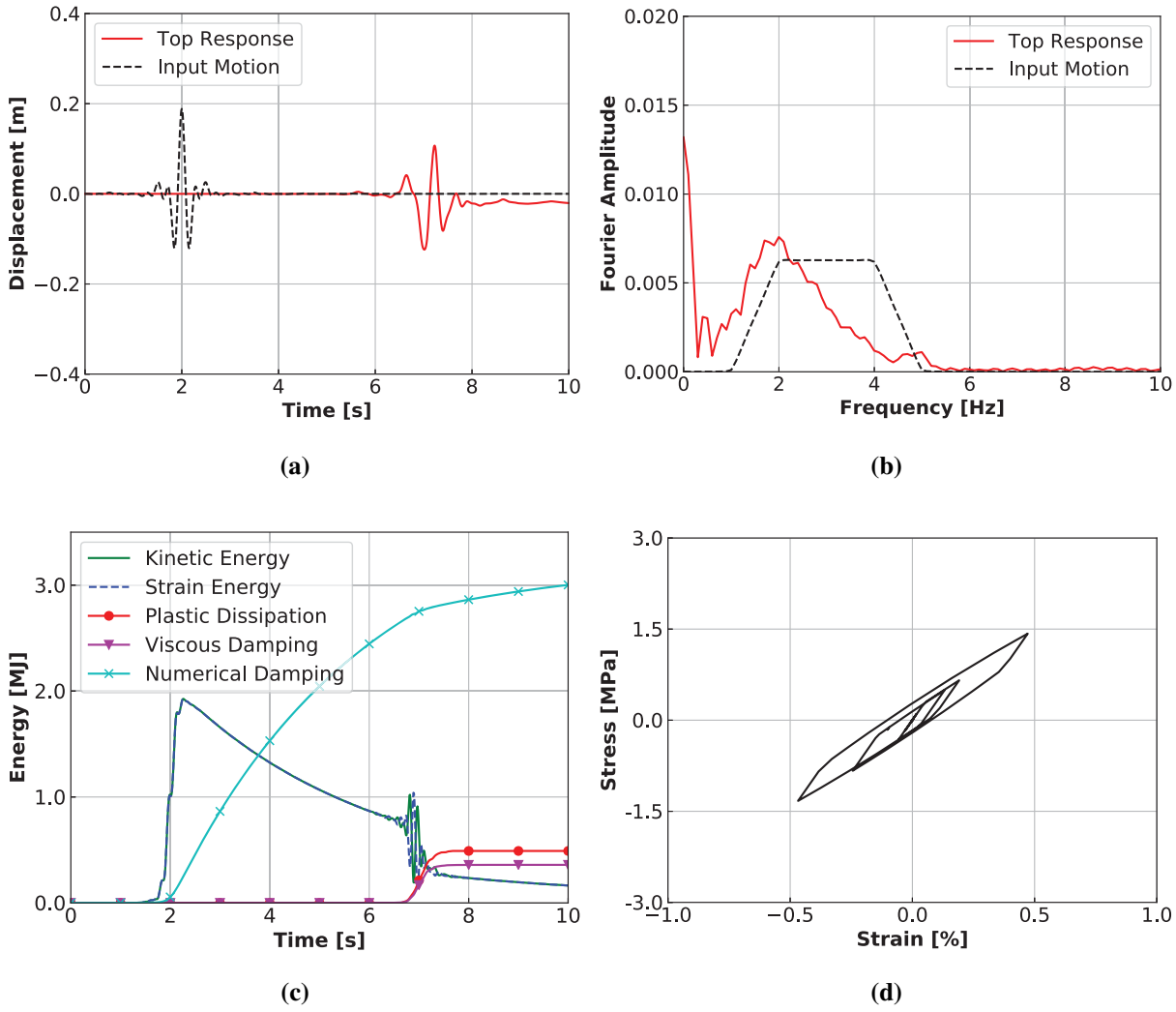

Fig. 24. Energy computation of wave propagation using medium inelastic material model, Rayleigh damping ($\xi = 0.04$), and algorithmic damping ($\gamma = 0.550$, $\beta = 0.276$): (a) Displacement time series; (b) Displacement spectrum; (c) Energy results; (d) Stress-strain response.